AIAA JOURNAL
Vol. 38, No. 12, December 2000

Geometrically Nonlinear Shell Element for Hygrothermorheologically Simple Linear Viscoelastic Composites

Daniel C. Hammerand* and Rakesh K. Kapania†
Virginia Polytechnic Institute and State University, Blacksburg, Virginia 24061-0203

A triangular flat shell element for large deformation analysis of linear viscoelastic laminated composites is presented. Hygrothermorheologically simple materials are considered for which a change in the hygrothermal environment results in a horizontal shifting of the relaxation moduli curves on a log timescale, in addition to the usual hygrothermal loads. Recurrence relations are developed and implemented for the evaluation of the viscoelastic memory loads. The nonlinear deformation process is computed using an incremental/iterative approach with the Newton–Raphson method used to find the incremental displacements in each time step. The presented numerical examples consider the large deformation and stability of linear viscoelastic structures under deformation-independent mechanical loads, deformation-dependent pressure loads, and thermal loads. Unlike elastic structures that have a single critical load value associated with a given snapping or buckling instability phenomenon, viscoelastic structures will usually exhibit a particular instability for a range of applied loads over a range of critical times. Both creep buckling and snap through examples are presented here. In some cases, viscoelastic results are also obtained using the quasi-elastic method in which load-history effects are ignored, and time-varying viscoelastic properties are simply used in a series of elastic problems. The presented numerical examples demonstrate the capability and accuracy of the formulation.

Introduction

In recent years, the use of composite materials has grown in popularity, because their response characteristics can be tailored to meet specific design requirements, while allowing structural components to remain lightweight. Usually, composite structures are analyzed using a linear elastic material law. However, a linear elastic analysis may give inaccurate results for fiber-reinforced polymer matrix composites because it is well known that polymers are viscoelastic in nature.[1] Furthermore, the viscoelastic response of polymers is affected by environmental conditions, such as temperature and moisture.[2,3]

Of the various techniques available to a structural analyst, perhaps the most useful is that of finite element analysis, due to its wide applicability to complex problems, the wide availability of commercial codes, and the low cost of computational resources at the present time. Even in the beginning of its growth in popularity, the finite element method was applied in analyzing viscoelastic structures.[4,5] The finite element method continues to be used regularly for the small-deformation response of isotropic and laminated linear viscoelastic structures.[6–16] For the regime of geometrically nonlinear response, most finite element research has been performed for the isotropic viscoelastic case,[17–23] whereas little work has been reported for the case of viscoelastic laminated composites.[24–27] However, additional research has been conducted on the large-deformation and stability analysis of viscoelastic composites using more traditional approaches.[28–35]

To determine the large deformations of structures using the finite element method, an incremental approach typically is used. Often, the second Piola–Kirchhoff (PK2) stress tensor is employed in conjunction with the nonlinear Green–Saint-Venant strain tensor in the description of the material behavior. Any known configuration can be used as the reference configuration for these tensors, which leads to two alternative methods. In the total Lagrangian method, the original configuration is chosen as the reference state, whereas in the updated Lagrangian method, the reference state is updated throughout the deformation process. As noted by Bathe,[36] the two approaches give identical results, provided that the constitutive laws used in each are equivalent.

Yang and Lianis[17] applied an incremental midpoint-tangent approach to study the quasi-static large-deflection behavior of isotropic linear viscoelastic beams and frames. In their finite element approach, linear strain–displacement relations were used in each increment, with the nodal coordinates updated at the end of each increment to account for the effects of geometric nonlinearity.

Key[18] developed a finite element method for the large-deflection dynamic analysis of axisymmetric solids. A linear relation was used between the PK2 stresses and the nonlinear Green–Saint-Venant strain histories, thereby restricting the accuracy of the formulation in most cases to large deflections/rotations but small strains.

Shen et al.[19] used a total Lagrangian approach in formulating a finite element code for the geometrically nonlinear dynamic response of axisymmetric and three-dimensional isotropic linear viscoelastic solids. The constant average acceleration method of the Newmark family was used in representing both the acceleration appearing in the inertia term and the time derivative of the strain occurring in the hereditary integral of the constitutive law.

Shen et al.[20] presented both a total Lagrangian and updated Lagrangian approach for the three-dimensional finite element analysis of isotropic viscoelastic solids. The material law was written for a total Lagrangian description. The resulting recursion relations derived for updating the stresses could be used directly in the total Lagrangian approach presented. However, to use these recursion relations in their updated Lagrangian approach, the recursion relations had to be transformed using the deformation gradient tensor from the original reference state to the current reference state. As will be shown in the present formulation, this additional complexity in the updated Lagrangian formulation can be avoided by judicious choice of the reference states used in developing recursion relations from the material law.

Roy and Reddy[21] analyzed the geometrically nonlinear deformations of adhesive joints using an updated Lagrangian finite element

Presented as Paper 99-1235 at the AIAA/ASME/ASCE/AHS/ASC 40th Structures, Structural Dynamics, and Materials Conference, St. Louis, MO, 12–15 April 1999; received 13 July 1999; revision received 11 May 2000; accepted for publication 12 May 2000.

*Graduate Assistant, Department of Aerospace and Ocean Engineering; currently Postdoctoral Appointee, Material Mechanics Department, Sandia National Laboratories, P.O. Box 5800, MS-0847, Albuquerque, NM 87185-0847. Student Member AIAA.

†Professor, Department of Aerospace and Ocean Engineering. Associate Fellow AIAA.

formulation. The adhesive was modeled as nonlinear viscoelastic using a constitutive law proposed by Schapery.[37]

Jenkins and Leonard[22] extended the method of White[4] to the case of geometrically nonlinear deformations to study the dynamic in-plane and transverse deformations of viscoelastic membranes. The numerical approximation of the viscoelastic material law was incorporated directly into the incremental finite element equations, which were cast in a total Lagrangian form.

Faria et al.[23] computed the rolling resistance moment of a steadily rolling viscoelastic cylinder using the finite element method. The finite-strain viscoelastic material law was based on the use of an internal state variable tensor. The history of this tensor was governed by a linear differential equation incorporating a single relaxation time. Because the formulation concerned only steady-state deformations, the resulting stress and strain histories for particles in a common band were known in terms of their respective circumferential distributions. Faria et al.[23] also studied the large deformations of a standard passenger tire. Those analyses involved the use of anisotropic layered shells, but whether an elastic or viscoelastic constitutive law was used was not explicitly stated, nor was it clear from the results presented.

In a three-part series of papers, Padovan,[24] Kennedy and Padovan,[25] and Nakajima and Padovan[26] used the finite element method to analyze the large deformations of viscoelastic rings, tori, and tires under external loads, contact, and friction. The viscoelastic constitutive behavior was expressed using fractional derivatives. The internal laminations present in tires were handled via Halpin–Tsai correlations (see Ref. 38). The Galilean transformation technique was used in developing a moving/rolling element method in which the material derivatives appearing in the rolling equations of motion are expressed as a local time derivative plus a purely spatial derivative. Steady-state deformations were analyzed using a hierarchically constrained Newton–Rapshon technique, whereas transient responses were determined using the Newmark method.

Marques and Creus[27] extended the linear elastic, total Lagrangian finite element formulation of Bathe[36] to include the effects of anisotropic hygrothermorheologically simple linear viscoelasticity. In the total Lagrangian formulation of Bathe,[36] the nonlinear terms in the principle of virtual work resulting from the product of the incremental PK2 stresses and the virtual nonlinear Green–Saint-Venant strains is linearized as follows. The virtual work of the incremental PK2 stresses is taken as the product of the incremental PK2 stresses and the virtual small-strain tensor. Also, the constitutive equation for the incremental PK2 stresses is linearized such that the incremental PK2 stress tensor depends only on the terms in the incremental strain tensor that are linear in the incremental displacements. The small- and large-deflection behavior of laminated graphite–epoxy plates and shells was studied. For a viscoelastic shell cap under a central point force that was applied as a creep load, that is, the load was applied suddenly and then held constant, the critical elapsed time to snap through was found to increase as the load magnitude decreased.

Using a quasi-elastic approach, Wilson and Vinson studied the linear viscoelastic buckling of laminated plates[28] and columns.[29] In the quasi-elastic method,[39] the current viscoelastic response is determined by simply using the viscoelastic properties corresponding to an elapsed time equal to the current time in an elastic analysis. Using the quasi-elastic method allowed the determination of the time variation of the viscoelastic buckling curve for creep loading by the solution of a series of elastic eigenvalue analyses. This viscoelastic buckling curve gives the magnitude of the creep loading applied at $t = 0$ necessary to cause buckling at a given time t. Hence, using the quasi-elastic method simplified the viscoelastic buckling problem considerably for situations where a similar elastic structure would undergo bifurcation buckling with no prebuckling deformation because viscoelastic stability was determined using eigenvalue analysis of geometrically perfect elastic structures. For the analysis of such problems using a full viscoelastic approach, it would be necessary to examine if an initial deflection (caused by an imperfection in the structure or its loading) grows large under a given loading. For both plates and columns, the viscoelastic stability curve was observed to decrease significantly (15% or more) as time evolved. The more prominent the matrix's role in the structural response, the more pronounced was the decay in the viscoelastic buckling load because the fibers were taken to be elastic, whereas the matrix was treated as viscoelastic.

Using the quasi-elastic method, Vinogradov[30] studied the viscoelastic buckling of asymmetric laminated beam columns composed of two layers of isotropic linear viscoelastic materials bonded together. A safe load limit that depended only on long-term creep compliance values and geometric parameters was determined. It appeared that the buckling characteristics could be enhanced by tailoring the laminate composition.

Kim and Hong[31] studied the viscoelastic buckling of sandwich plates with cross-ply faces using the quasi-elastic approach. The core was assumed to be elastic, whereas both the adhesive and the surface plates were taken to be linear viscoelastic. The in-plane viscoelastic buckling load varied with the face stacking sequence, adhesive strength, plate aspect ratio, and biaxial load ratio.

Huang studied the linear viscoelastic response of imperfect composite plates[32] and cylindrical panels[33] under in-plane compressive loads. The Laplace transform of the compatibility equation was used to determine the viscoelastic stress function. The transverse deflection was found by applying Galerkin's method to the moment equation. Using a similar approach, quasi-elastic estimates for the viscoelastic deformation were also determined. The edge loads were applied as creep loads at $t = 0$ in each case considered. However, because the internal moments depended on the edge loads and the transverse deflections, the internal loading was time dependent. The time history of viscoelastic deflection for both plates and cylindrical panels was shown to be sensitive to the size of the initial imperfection. For various combinations of loading and initial imperfection magnitudes, viscoelastic buckling occurred in the plates, whereas viscoelastic snap through resulted for some of the cylindrical panels. Although the accuracy of the quasi-elastic method was acceptable in some cases, in general, it overestimated the growth of the viscoelastic deflections and underestimated the critical times for buckling or snapping. These trends resulted because the quasi-elastic method finds the current viscoelastic deflection by considering the internal load history to be the current internal loads applied as creep loads at $t = 0$.

Touati and Cederbaum[34] used Schapery's nonlinear viscoelastic material law[37] in studying the postbuckling response of laminated plates with initial imperfections. The nonlinear equilibrium equations were solved by first transforming them into a system of first-order nonlinear differential equations, which were then solved using Galerkin's method in conjunction with a higher-order Runge–Kutta method.

Shalev and Aboudi[35] used higher-order shear deformation theory to study the postbuckling response of symmetric cross-ply laminated plates. Only creep loads large enough to cause instantaneous buckling of the viscoelastic plates were applied. The linear viscoelastic solution was developed using the correspondence principle[40] to find the solution in the Laplace domain. Numerical inversion was used to determine the time-domain solution.

The geometrically nonlinear formulation of a triangular flat shell element for linear elastic laminated composite structures[41] is extended here to model hygrothermorheologically simple linear viscoelastic composites. In addition to the derivation of the internal force vector and tangent stiffness matrix, details of the iterative technique are also given. Deformation-independent mechanical loads, deformation-dependent pressure loads, and hygrothermal loads can be applied simultaneously. Numerical examples are presented to validate the formulation and to examine the large-deformation response and stability of viscoelastic structures.

Triangular Flat Shell Element Overview

Flat shell elements are obtained as the superposition of a membrane and a bending element. The shell behavior (geometric coupling of membrane and bending behaviors) results between elements from transforming the element stiffness matrices and load vectors to a single global coordinate system. The present flat shell element combines the discrete-Kirchhoff theory (DKT) plate bending element (see Ref. 42) with a membrane element having the same nodal degrees of freedom (DOF) as the Allman triangle (AT).[43]

The DKT plate bending element begins with shape functions for the rotations of the normal to the undeformed midsurface. The assumption of thin structures is incorporated in two ways. First, the transverse shear energy is neglected so that the strain energy is only that resulting from bending. Second, the Kirchhoff hypothesis that the transverse shear is zero is applied along the edges of the element.

Following Ertas et al.,[44] the transformation suggested by Cook[45] is used to transform the well-known linear strain triangle (LST) element into a membrane element having two in-plane translational DOF and one drilling DOF at each node. The in-plane strain–displacement relations are derived as follows. The LST shape functions are used to derive the strain–displacement relations in terms of the DOF of the LST element. The resulting relations are then expressed in terms of the DOF of the AT by mapping the two in-plane translational DOF at the midside nodes of the LST element into in-plane translational and drilling DOF at the corner nodes.[41,46]

Altogether, the triangular flat shell element has three translations and three rotations at each corner node for a total of 18 DOF. The geometrically nonlinear formulation of this element for the linear elastic case was presented by Mohan and Kapania,[41] whereas the geometrically linear formulation of this element for the thermoviscoelastic case was presented by Hammerand and Kapania.[16] Henceforth, the geometrically nonlinear, linear elastic element will be referred to as Allman triangle, discrete Kirchhoff theory triangle, nonlinear (ATDKT-NL), whereas the present linear viscoelastic extension to this element will be termed TVATDKT-NL.

Newton–Raphson Method

Throughout this work, left-hand superscripts will be used to denote the configuration in which a quantity occurs, whereas left-hand subscripts will be used to denote the configuration in which the quantity is measured. For instance, the global internal force vector $\{F_{\text{int}}\}$, occurring at time t^p but measured in the configuration corresponding to time t^{p-1} is denoted as $\{{}_{p-1}{}^{p}F_{\text{int}}\}$.

Assuming that the equilibrium state at time t^{p-1} is known, the incremental equations needed for the determination of the equilibrium state at time t^p are developed using the Newton–Raphson method. In the present formulation, the only external load that is taken to be deformation dependent is the pressure load $\{F_P\}$. Hence, $\{\Delta U^{(n+1)}\}$, the change in the incremental displacements $\{U\}$ from iteration (n) to iteration $(n+1)$, is obtained by solving

$$\left[K_T^{(n)} - K_P^{(n)}\right]\left\{\Delta U^{(n+1)}\right\} = \left\{{}_{p-1}{}^{p}F_{\text{ext}}\left(\left\{U^{(n)}\right\}\right)\right\} - \left\{{}_{p-1}{}^{p}F_{\text{int}}\left(\left\{U^{(n)}\right\}\right)\right\} \tag{1}$$

where $[K_T]$ is the global tangent stiffness matrix given by

$$[K_T] = \frac{\partial\{F_{\text{int}}\}}{\partial\{U\}} \tag{2}$$

and $[K_P]$ is the global pressure stiffness matrix given by

$$[K_P] = \frac{\partial\{F_P\}}{\partial\{U\}} \tag{3}$$

and $\{F_{\text{ext}}\}$ is the global external load vector considering all applied loads. The derivation of the deformation-dependent pressure load $\{F_p\}$ and pressure stiffness matrix $[K_p]$ is presented in Ref. 47. Because neither $\{F_p\}$ nor $[K_p]$ involves material properties, no modifications are necessary to use these quantities when modeling linear viscoelastic composite structures. Quantities corresponding to $[K_T]$, $[K_P]$, $\{U\}$, $\{F_{\text{ext}}\}$, and $\{F_{\text{int}}\}$ for an element will be denoted with the corresponding lowercase letters.

Derivation of the Internal Force Vector

The internal force vector $\{f_{\text{int}}\}$ for an element is derived from the following expression for the internal virtual work δW_{int}:

$$\delta W_{\text{int}} = \{\delta u\}^T\left\{{}_{p-1}{}^{p}f_{\text{int}}\right\} = \int_{A^{p-1}}\int_{z_{\min}}^{z_{\max}}\left\{\delta_{p-1}{}^{p}\epsilon\right\}^T\left\{{}_{p-1}{}^{p}S\right\}\,\mathrm{d}z\,\mathrm{d}A^{p-1} \tag{4}$$

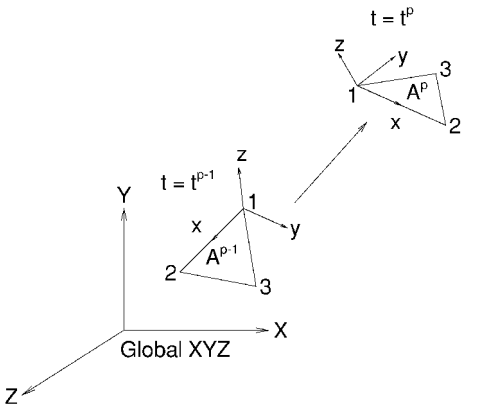

Fig. 1 Deformation of a triangular flat shell element from time t^{p-1} to time t^p.

where $\{{}_{p-1}{}^{p}\epsilon\}$ is the vector of total Green–Saint-Venant strains, $\{{}_{p-1}{}^{p}S\}$ is the vector of PK2 stresses, A^{p-1} refers to the area of the element at time t^{p-1}, and z is the local through-the-thickness coordinate. Note that $\{{}_{p-1}{}^{p}\epsilon\}$ and $\{{}_{p-1}{}^{p}S\}$ can be expressed in component form for any defined coordinate system. In the present formulation for each element, they are expressed in a local coordinate system defined by the element geometry at time t^{p-1}. The reason for this choice will become clear later in the formulation. At any given time, an element has the following local coordinate system: The local x axis is aligned with side 1–2 of the element, the local y axis lies in the plane of the element, and the local z axis points in the direction of the normal to the element. An element undergoing deformation from t^{p-1} to t^p is shown in Fig. 1. The local coordinate systems for the element at times t^{p-1} and t^p are also indicated.

Assuming thin shells undergoing moderate incremental rotations, the total Green–Saint-Venant strains are written as

$$\left\{{}_{p-1}{}^{p}\epsilon\right\} = \left\{{}_{p-1}{}^{p}e\right\} + z\left\{{}_{p-1}{}^{p}\kappa\right\} \tag{5}$$

where $\{{}_{p-1}{}^{p}e\}$ and $\{{}_{p-1}{}^{p}\kappa\}$, respectively, denote the total midsurface in-plane strains and bending curvatures. The variation in the vector of Green–Saint-Venant strains is then

$$\left\{\delta_{p-1}{}^{p}\epsilon\right\} = \left\{\delta_{p-1}{}^{p}e\right\} + z\left\{\delta_{p-1}{}^{p}\kappa\right\} \tag{6}$$

The incremental midplane strains $\{\Delta_{p-1}{}^{p}e\}$ and bending curvatures $\{\Delta_{p-1}{}^{p}\kappa\}$ are given in terms of the incremental deformations as

$$\left\{\Delta_{p-1}{}^{p}e\right\} = \left\{{}_{p-1}{}^{p}e\right\} - \left\{{}_{p-1}{}^{p-1}e\right\} = \begin{Bmatrix} u_{,x} + 1/2\left(u_{,x}^2 + v_{,x}^2 + w_{,x}^2\right) \\ v_{,y} + 1/2\left(u_{,y}^2 + v_{,y}^2 + w_{,y}^2\right) \\ u_{,y} + v_{,x} + u_{,x}u_{,y} + v_{,x}v_{,y} + w_{,x}w_{,y} \end{Bmatrix} \tag{7}$$

$$\left\{\Delta_{p-1}{}^{p}\kappa\right\} = \left\{{}_{p-1}{}^{p}\kappa\right\} - \left\{{}_{p-1}{}^{p-1}\kappa\right\} = \{\beta_{x,x} \quad \beta_{y,y} \quad (\beta_{x,y} + \beta_{y,x})\}^T \tag{8}$$

where u, v, and w are the incremental midplane translations; β_x and β_y are the incremental rotations of the midplane normal about the positive local y and negative x axes, respectively; and subscripts $,x$ and $,y$, respectively, denote $\partial(\cdot)/\partial x$ and $\partial(\cdot)/\partial y$.

In terms of the incremental nodal displacements, the spatial derivatives of the incremental displacements for an element are written as[41]

$$\{u_{,x} \quad u_{,y} \quad v_{,x} \quad v_{,y} \quad w_{,x} \quad w_{,y}\}^T = [G_2]\{u\} \tag{9}$$

The incremental in-plane strains are then easily determined using Eq. (7). The incremental bending curvatures are written in terms of the incremental nodal displacements as[41]

$$\left\{\Delta_{p-1}{}^{p}\kappa\right\} = [B_{\text{DKT}}]\{u\} \tag{10}$$

At a given location within an element, $[G_2]$ and $[B_{\mathrm{DKT}}]$ depend only on the nodal coordinates of the element at the end of the last fully converged time step. The variations of the in-plane strains and bending curvatures can be written in terms of the variations of the incremental nodal displacements as

$$\left\{\delta_{p-1}^{\ p}e\right\} = [G_1(\{u\})][G_2]\{\delta u\} \tag{11}$$

$$\left\{\delta_{p-1}^{\ p}\kappa\right\} = [B_{\mathrm{DKT}}]\{\delta u\} \tag{12}$$

where $[G_1]$ is given by

$$[G_1] = \begin{bmatrix} 1+u_{,x} & 0 & v_{,x} & 0 & w_{,x} & 0 \\ 0 & u_{,y} & 0 & 1+v_{,y} & 0 & w_{,y} \\ u_{,y} & 1+u_{,x} & 1+v_{,y} & v_{,x} & w_{,y} & w_{,x} \end{bmatrix} \tag{13}$$

The current force resultant $\{_{p-1}^{\ p}N\}$ and force-couple resultant $\{_{p-1}^{\ p}M\}$ are defined as

$$\left\{_{p-1}^{\ p}N\right\} = \int_{z_{\min}}^{z_{\max}} \left\{_{p-1}^{\ p}S\right\} \mathrm{d}z \tag{14}$$

$$\left\{_{p-1}^{\ p}M\right\} = \int_{z_{\min}}^{z_{\max}} z\left\{_{p-1}^{\ p}S\right\} \mathrm{d}z \tag{15}$$

Although $\{N\}$ and $\{M\}$ are here termed force resultant and force-couple resultant, respectively, note that $\{N\}$ and $\{M\}$ have little physical meaning because they are based on integrating PK2 pseudostresses through the thickness.

Using Eqs. (4), (6), (11), (12), (14), and (15), the internal force vector for an element is determined to be

$$\left\{_{p-1}^{\ p}f_{\mathrm{int}}\right\} = \int_{A^{p-1}} \left([G_2]^T[G_1]^T\left\{_{p-1}^{\ p}N\right\} + [B_{\mathrm{DKT}}]^T\left\{_{p-1}^{\ p}M\right\}\right) \mathrm{d}A^{p-1} \tag{16}$$

Derivation of Force and Force-Couple Resultants

The current PK2 stresses are written in the following incremental form:

$$\left\{_{p-1}^{\ p}S\right\} = \left\{_{p-1}^{\ p-1}S\right\} + \left\{\Delta_{p-1}^{\ p}S\right\} \tag{17}$$

Note that $\{_{p-1}^{\ p-1}S\}$ is actually a vector of Cauchy stresses. Obviously, after an increment has been converged, it will be necessary to transform the PK2 stress $\{_{p-1}^{\ p}S\}$ into the Cauchy stress $\{_{p}^{\ p}S\}$ to be used for the next increment. This transformation is performed using the deformation gradient tensor.[36] However, for the case of small incremental strains, it can be shown that the current PK2 stress ($\{_{p-1}^{\ p}S\}$) expressed in the local coordinate system corresponding to the element at time t^{p-1} is approximately equal to the current Cauchy stress ($\{_{p}^{\ p}S\}$) expressed in the local coordinate system corresponding to the element at time t^p (Ref. 48). This approximation was successfully employed by Mohan and Kapania[41] and will be used here also.

For the class of materials that are called hygrothermorheologically simple, changing the temperature and/or moisture results in a simple horizontal shifting of the relaxation moduli on a log timescale. For such materials in the one-dimensional isotropic case, the relaxation modulus E at the physical temperature T, moisture H, and time t can be related to the relaxation modulus at the reference temperature T_{ref}, reference moisture H_{ref}, and reduced time ζ by

$$E(T, H, t) = E(T_{\mathrm{ref}}, H_{\mathrm{ref}}, \zeta) \tag{18}$$

where the reduced time and physical time are related by the horizontal shift factor A_{TH} as follows:

$$\zeta = \int_0^t \frac{\mathrm{d}t'}{A_{TH}[T(t'), H(t')]} \tag{19}$$

For the case of a hygrothermorheologically simple, linear viscoelastic composite material, the stress and strain are related as follows:

$$\left\{_{p-1}^{\ p}S\right\} = \int_0^{t^p} [\bar{Q}(\zeta^p - \zeta')]\left\{\frac{\partial_{p-1}^{\ \tau}\epsilon}{\partial\tau}\right\} \mathrm{d}\tau \tag{20}$$

$$\left\{_{p-1}^{\ p-1}S\right\} = \int_0^{t^{p-1}} [\bar{Q}(\zeta^{p-1} - \zeta')]\left\{\frac{\partial_{p-1}^{\ \tau}\epsilon}{\partial\tau}\right\} \mathrm{d}\tau \tag{21}$$

where $[\bar{Q}(t)]$ is the matrix of relaxation moduli and $\{_{p-1}^{\ \tau}\epsilon\}$ represents the vector of total mechanical strains up to time τ. These mechanical strains are given in terms of the corresponding total strains as

$$\begin{aligned}\left\{_{p-1}^{\ \tau}\epsilon\right\} &= \left\{_{p-1}^{\ \tau}\epsilon\right\} - \theta_T^\tau\{\alpha\} - \theta_H^\tau\{\bar{\beta}\} \\ &= \left\{_{p-1}^{\ \tau}e\right\} + z\left\{_{p-1}^{\ \tau}\kappa\right\} - \theta_T^\tau\{\alpha\} - \theta_H^\tau\{\bar{\beta}\}\end{aligned} \tag{22}$$

where θ_T^τ and θ_H^τ are the deviation of the temperature and moisture from the thermal and hygroscopic strain-free states at time τ, respectively, and $\{\alpha\}$ and $\{\bar{\beta}\}$ are the transformed coefficients of thermal and hygroscopic expansion, respectively. Both the temperature and moisture are assumed to be uniform through the thickness of the laminate, whereas the coefficients of thermal and hygroscopic expansion depend on the fiber orientation of the layer being considered. In Eqs. (20) and (21), the reduced times ζ^p and ζ^{p-1} correspond to t^p and t^{p-1}, respectively, and the reduced time ζ' corresponds to τ. Also note that in Eqs. (20) and (21), the strains for all past history are referred to the known configuration corresponding to time t^{p-1}. This choice will simplify the resulting expressions for the incremental PK2 stresses.

Each layer of the laminate is assumed to be orthotropic and made of the same material so that four relaxation moduli (Q_{11}, Q_{12}, Q_{22}, and Q_{66}) describe the laminate material behavior. The following contracted notation is used for the relaxation moduli:

$$Q_1 = Q_{11}, \qquad Q_2 = Q_{12}, \qquad Q_3 = Q_{22}, \qquad Q_4 = Q_{66} \tag{23}$$

Each relaxation modulus is expressed in terms of a Prony series as follows:

$$Q_r(t) = Q_r^\infty + \sum_{\rho=1}^{N_r} Q_{r\rho}\exp\left(-\frac{t}{\lambda_{r\rho}}\right) \qquad \text{for } r = 1, 2, 3, 4 \tag{24}$$

where the $\lambda_{r\rho}$ denote relaxation times governing the material response characteristics. Each reduced stiffness is allowed to have its own reduced timescale denoted by ζ_r to model the possibility that it may be affected differently by the hygrothermal environment. The matrix of relaxation moduli in the material law can then be written as

$$\begin{aligned}[\bar{Q}(\zeta^p - \zeta')] &= \sum_{r=1}^{4} Q_r\left(\zeta_r^p - \zeta_r'\right)[D_r] \\ &= \sum_{r=1}^{4}\left[Q_r^\infty + \sum_{\rho=1}^{N_r} Q_{r\rho}\exp\left(-\frac{\zeta_r^p - \zeta_r'}{\lambda_{r\rho}}\right)\right][D_r]\end{aligned} \tag{25}$$

where

$$\zeta_r^p = \int_0^{t^p} \frac{\mathrm{d}t'}{A_r[T(t'), H(t')]}, \qquad \zeta_r' = \int_0^{\tau} \frac{\mathrm{d}t'}{A_r[T(t'), H(t')]} \tag{26}$$

Note that $[D_i]$ is the transformed reduced stiffness matrix for the elastic case with $Q_i = 1$ and the other three Q_r equal to zero.

The current PK2 stresses are determined as

$$\left\{_{p-1}^{\ p}S\right\} = \sum_{r=1}^{4} Q_r^\infty[D_r]\left\{_{p-1}^{\ p}\epsilon\right\} + \sum_{r=1}^{4}\sum_{\rho=1}^{N_r}\left\{_{p-1}^{\ p}V_{r\rho}\right\} \tag{27}$$

where

$$\left\{{}_{p-1}^{p}V_{r\rho}\right\} = \int_0^{t^p} Q_{r\rho}\exp\left(-\frac{\zeta_r^p - \zeta_r^l}{\lambda_{r\rho}}\right)[D_r]\left\{\frac{\partial_{p-1}^{\tau}\bar{\epsilon}}{\partial\tau}\right\}\mathrm{d}\tau \quad (28)$$

Likewise, the PK2 stresses at the end of the last time increment are

$$\left\{{}_{p-1}^{p-1}S\right\} = \sum_{r=1}^{4} Q_r^{\infty}[D_r]\left\{{}_{p-1}^{p-1}\bar{\epsilon}\right\} + \sum_{r=1}^{4}\sum_{\rho=1}^{N_r}\left\{{}_{p-1}^{p-1}V_{r\rho}\right\} \quad (29)$$

Writing the expression for $\{{}_{p-1}^{p-1}V_{r\rho}\}$ and evaluating the hereditary integral over t^{p-1} to t^p by approximating $\{\partial_{p-1}^{\tau}\bar{\epsilon}/\partial\tau\}$ to be constant over the time step, the following recurrence relation is obtained for $\{{}_{p-1}^{p}V_{r\rho}\}$:

$$\left\{{}_{p-1}^{p}V_{r\rho}\right\} = \exp\left[-\left(\Delta\zeta_r^p/\lambda_{r\rho}\right)\right]\left\{{}_{p-1}^{p-1}V_{r\rho}\right\} + \bar{S}_{r\rho}^p Q_{r\rho}[D_r]\left\{\Delta_{p-1}^{p}\bar{\epsilon}\right\} \quad (30)$$

where $\bar{S}_{r\rho}^p$ is defined as

$$\bar{S}_{r\rho}^p = \frac{1}{\Delta t^p}\int_{t^{p-1}}^{t^p}\exp\left(-\frac{\zeta_r^p - \zeta_r^l}{\lambda_{r\rho}}\right)\mathrm{d}\tau \quad (31)$$

For the case where A_r is constant over a time step, $\bar{S}_{r\rho}^p$ can be evaluated exactly as[5]

$$\bar{S}_{r\rho}^p = \frac{1}{\Delta\zeta_r^p}\lambda_{r\rho}\left[1 - \exp\left(-\frac{\Delta\zeta_r^p}{\lambda_{r\rho}}\right)\right] \quad (32)$$

Taylor et al.[5] demonstrated the importance of accurately evaluating $\bar{S}_{r\rho}^p$ in controlling numerical error. Presumably, a sufficiently small time step size will be used so that Eq. (32) represents an acceptable approximation to Eq. (31) for a given variation in the hygrothermal environment.

Using Eqs. (27), (29), and (30), the incremental PK2 stresses $\{\Delta_{p-1}^{p}S\}$ are given by

$$\left\{\Delta_{p-1}^{p}S\right\} = \sum_{r=1}^{4}\left[Q_r^{\infty} + \sum_{\rho=1}^{N_r}\bar{S}_{r\rho}^p Q_{r\rho}\right][D_r]\left\{\Delta_{p-1}^{p}\bar{\epsilon}\right\} - \sum_{r=1}^{4}\sum_{\rho=1}^{N_r}\left[1 - \exp\left(-\frac{\Delta\zeta_r^p}{\lambda_{r\rho}}\right)\right]\left\{{}_{p-1}^{p-1}V_{r\rho}\right\} \quad (33)$$

The first term gives the incremental PK2 stresses resulting from the current incremental strains, whereas the second term gives the change in the PK2 stresses resulting from the relaxation over the current time step of the stresses corresponding to the strains that occurred up to the end of the previous time step.

The current force and force-couple resultants are determined by using Eq. (33) in

$$\left\{{}_{p-1}^{p}N;\ {}_{p-1}^{p}M\right\} = \int_{z_{\min}}^{z_{\max}}(1;\ z)\left(\left\{{}_{p-1}^{p-1}S\right\} + \left\{\Delta_{p-1}^{p}S\right\}\right)\mathrm{d}z \quad (34)$$

Using the decomposition of the mechanical Green–Saint-Venant strains given by Eq. (22), the current force resultant is, thus,

$$\left\{{}_{p-1}^{p}N\right\} = \left\{{}_{p-1}^{p-1}N\right\} - \sum_{r=1}^{4}\sum_{\rho=1}^{N_r}\left[1 - \exp\left(-\frac{\Delta\zeta_r^p}{\lambda_{r\rho}}\right)\right]\left\{{}_{p-1}^{p-1}N_{r\rho}\right\} + [\tilde{A}^p]\left\{\Delta_{p-1}^{p}e\right\} + [\tilde{B}^p]\left\{\Delta_{p-1}^{p}\kappa\right\} - \sum_{r=1}^{4}\left[Q_r^{\infty} + \sum_{\rho=1}^{N_r}\bar{S}_{r\rho}^p Q_{r\rho}\right] \times\left(\Delta\theta_T^p\left\{N_r^T\right\} + \Delta\theta_H^p\left\{N_r^H\right\}\right) \quad (35)$$

where

$$[\tilde{A}^p;\ \tilde{B}^p;\ \tilde{D}^p] = \sum_{r=1}^{4}\left[Q_r^{\infty} + \sum_{\rho=1}^{N_r}\bar{S}_{r\rho}^p Q_{r\rho}\right][\bar{A}_r;\ \bar{B}_r;\ \bar{D}_r] \quad (36)$$

$$[\bar{A}_r;\ \bar{B}_r;\ \bar{D}_r] = \int_{z_{\min}}^{z_{\max}}(1;\ z;\ z^2)[D_r]\,\mathrm{d}z \quad (37)$$

$$\left\{{}_{p-1}^{p-1}N_{r\rho}\right\} = \int_{z_{\min}}^{z_{\max}}\left\{{}_{p-1}^{p-1}V_{r\rho}\right\}\mathrm{d}z \quad (38)$$

$$\left\{N_r^T\right\} = \int_{z_{\min}}^{z_{\max}}[D_r]\{\alpha\}\,\mathrm{d}z \quad (39)$$

$$\left\{N_r^H\right\} = \int_{z_{\min}}^{z_{\max}}[D_r]\{\bar{\beta}\}\,\mathrm{d}z \quad (40)$$

Note that for the case where all $Q_{r\rho}$ are equal to zero, $[\tilde{A}^p;\ \tilde{B}^p;\ \tilde{D}^p]$ reduce to the usual matrices $[A;\ B;\ D]$ corresponding to an elastic laminate with reduced stiffnesses $Q_1^{\infty} - Q_4^{\infty}$.

Likewise, the current force-couple resultant is

$$\left\{{}_{p-1}^{p}M\right\} = \left\{{}_{p-1}^{p-1}M\right\} - \sum_{r=1}^{4}\sum_{\rho=1}^{N_r}\left[1 - \exp\left(-\frac{\Delta\zeta_r^p}{\lambda_{r\rho}}\right)\right]\left\{{}_{p-1}^{p-1}M_{r\rho}\right\} + [\tilde{B}^p]\left\{\Delta_{p-1}^{p}e\right\} + [\tilde{D}^p]\left\{\Delta_{p-1}^{p}\kappa\right\} - \sum_{r=1}^{4}\left[Q_r^{\infty} + \sum_{\rho=1}^{N_r}\bar{S}_{r\rho}^p Q_{r\rho}\right]\left(\Delta\theta_T^p\left\{M_r^T\right\} + \Delta\theta_H^p\left\{M_r^H\right\}\right) \quad (41)$$

where

$$\left\{{}_{p-1}^{p-1}M_{r\rho}\right\} = \int_{z_{\min}}^{z_{\max}} z\left\{{}_{p-1}^{p-1}V_{r\rho}\right\}\mathrm{d}z \quad (42)$$

$$\left\{M_r^T\right\} = \int_{z_{\min}}^{z_{\max}} z[D_r]\{\alpha\}\,\mathrm{d}z \quad (43)$$

$$\left\{M_r^H\right\} = \int_{z_{\min}}^{z_{\max}} z[D_r]\{\bar{\beta}\}\,\mathrm{d}z \quad (44)$$

Hence, the current force and force-couple resultants are equal to the summation of their previous values, some viscoelastic memory loads, and terms corresponding to the current incremental strains. The viscoelastic memory loads account for the relaxation over the current time step of the force and force-couple resultants corresponding to the strains that occurred up to the end of the previous time step. The factor $\bar{S}_{r\rho}^p$ that appears in the $[\tilde{A}^p;\ \tilde{B}^p;\ \tilde{D}^p]$ matrices and the hygrothermal terms accounts for the relaxation over the current time step of the force and force-couple resultants corresponding to the current incremental strains. Recall that the factor $\bar{S}_{r\rho}^p$ as defined by Eq. (31) resulted from assuming the current incremental strains to vary linearly over the current time step.

Based on Eq. (30), recursion relations are written for $\{{}_{p-1}^{p}N_{r\rho}\}$ and $\{{}_{p-1}^{p}M_{r\rho}\}$ as follows:

$$\left\{{}_{p-1}^{p}N_{r\rho}\right\} = \exp\left(-\Delta\zeta_r^p/\lambda_{r\rho}\right)\left\{{}_{p-1}^{p-1}N_{r\rho}\right\} + \bar{S}_{r\rho}^p Q_{r\rho}\left([\bar{A}_r]\left\{\Delta_{p-1}^{p}e\right\} + [\bar{B}_r]\left\{\Delta_{p-1}^{p}\kappa\right\} - \Delta\theta_T^p\left\{N_r^T\right\} - \Delta\theta_H^p\left\{N_r^H\right\}\right) \quad (45)$$

$$\left\{{}_{p-1}^{p}M_{r\rho}\right\} = \exp\left(-\Delta\zeta_r^p/\lambda_{r\rho}\right)\left\{{}_{p-1}^{p-1}M_{r\rho}\right\} + \bar{S}_{r\rho}^p Q_{r\rho}\left([\bar{B}_r]\left\{\Delta_{p-1}^{p}e\right\} + [\bar{D}_r]\left\{\Delta_{p-1}^{p}\kappa\right\} - \Delta\theta_T^p\left\{M_r^T\right\} - \Delta\theta_H^p\left\{M_r^H\right\}\right) \quad (46)$$

Derivation of the Tangent Stiffness Matrix

The elemental tangent stiffness matrix $[k_T]$ is determined by taking the variation of the elemental internal force vector and recognizing that

$$\left\{\delta_{p-1}^{p}f_{\mathrm{int}}\right\} = \frac{\partial\left\{{}_{p-1}^{p}f_{\mathrm{int}}\right\}}{\partial\{u\}}\{\delta u\} = [k_T]\{\delta u\} \quad (47)$$

Based on Eq. (16), the variation in $\{{}_{p-1}{}^{p}f_{\text{int}}\}$ is

$$\left\{\delta\,{}_{p-1}{}^{p}f_{\text{int}}\right\} = \int_{A^{p-1}} \left([G_2]^T[G_1]^T\left\{\delta\,{}_{p-1}{}^{p}N\right\} + [B_{\text{DKT}}]^T\left\{\delta\,{}_{p-1}{}^{p}M\right\} + [G_2]^T[\delta G_1]^T\left\{{}_{p-1}{}^{p}N\right\}\right) \mathrm{d}A^{p-1} \tag{48}$$

The last term occurs because $[G_1]$ depends on the incremental displacements. This term can be shown to be

$$[G_2]^T[\delta G_1]^T\left\{{}_{p-1}{}^{p}N\right\} = [G_2]^T\begin{bmatrix}\mathcal{N} & 0 & 0\\ 0 & \mathcal{N} & 0\\ 0 & 0 & \mathcal{N}\end{bmatrix}[G_2]\{\delta u\} \tag{49}$$

where

$$[\mathcal{N}] = \begin{bmatrix} {}_{p-1}{}^{p}N_x & {}_{p-1}{}^{p}N_{xy}\\ {}_{p-1}{}^{p}N_{xy} & {}_{p-1}{}^{p}N_y\end{bmatrix} \tag{50}$$

$$\left\{{}_{p-1}{}^{p}N\right\} = \begin{Bmatrix} {}_{p-1}{}^{p}N_x\\ {}_{p-1}{}^{p}N_y\\ {}_{p-1}{}^{p}N_{xy}\end{Bmatrix} \tag{51}$$

Recall that the temperature and moisture histories are taken to be prescribed; the variations in $\{{}_{p-1}{}^{p}N\}$ and $\{{}_{p-1}{}^{p}M\}$ are simply

$$\left\{\delta\,{}_{p-1}{}^{p}N\right\} = [\tilde{A}^p][G_1][G_2]\{\delta u\} + [\tilde{B}^p][B_{\text{DKT}}]\{\delta u\} \tag{52}$$

$$\left\{\delta\,{}_{p-1}{}^{p}M\right\} = [\tilde{B}^p][G_1][G_2]\{\delta u\} + [\tilde{D}^p][B_{\text{DKT}}]\{\delta u\} \tag{53}$$

The elemental tangent stiffness matrix is finally determined as

$$[k_T] = \int_{A^{p-1}} \left([G_2]^T[G_1]^T[\tilde{A}^p][G_1][G_2] + [G_2]^T[G_1]^T[\tilde{B}^p][B_{\text{DKT}}] + [B_{\text{DKT}}]^T[\tilde{B}^p][G_1][G_2] + [B_{\text{DKT}}]^T[\tilde{D}^p][B_{\text{DKT}}] + [G_2]^T\begin{bmatrix}\mathcal{N} & 0 & 0\\ 0 & \mathcal{N} & 0\\ 0 & 0 & \mathcal{N}\end{bmatrix}[G_2]\right) \mathrm{d}A^{p-1} \tag{54}$$

If all $Q_{r\rho} = 0$, then the $[\tilde{A}^p;\ \tilde{B}^p;\ \tilde{D}^p]$ matrices are equal to the usual $[A;\ B;\ D]$ matrices and the tangent stiffness matrix reduces, as it should, to the elastic case as presented by Mohan and Kapania.[41] For the linear viscoelastic case, the $[\tilde{A}^p;\ \tilde{B}^p;\ \tilde{D}^p]$ matrices are used to account for the relaxation over the current time step of the portion of the internal force corresponding to the current incremental strains.

Because the tangent stiffness matrix from each element needs to be calculated in each iteration (full Newton–Raphson method) or every few iterations (modified Newton–Raphson method), incorporating a different set of reduced timescales for each element is not overly cumbersome. Hence, each element is allowed to be at its own temperature and moisture in the present formulation, which allows structures with nonuniform, time-dependent hygrothermal fields to be analyzed. For the case of nonuniform hygrothermal fields, an element's temperature and moisture will be approximated as the average of its nodal values. Obviously, the mesh size needed for convergence will depend on the the spatial distribution of the temperature and moisture throughout the time period of interest.

Note that using a single temperature and moisture for each element at each discrete time considered is consistent with the use of Eq. (22), which assumes that neither the temperature nor the moisture varies through the thickness of the structure. To model hygrothermal gradients in the thickness direction, the formulation would have to be modified significantly to account for the variation through the thickness of the reduced timescales. If the gradients in the thickness direction are large enough, a single set of reduced timescales for each layer may not be sufficient. For such cases, the individual layers may be divided into sublayers with independent reduced timescales.

Details of the Iterative Technique

The full Newton–Raphson method will be used such that the change in the incremental displacements for iteration $(n+1)$ is determined by solving Eq. (1). Before assembly, the elemental internal force vector, tangent stiffness matrix, pressure load, and pressure stiffness matrix are all transformed to the global coordinate system using the standard transformation techniques. All integrals over the area of an element are evaluated using a three-point rule in area coordinates.[49]

For an element in the first iteration of a time step $(n+1=1)$, the viscoelastic memory and incremental hygrothermal loads are applied so that the internal force vector $\{{}_{p-1}{}^{p}f_{\text{int}}^{(0)}\}$ is computed using

$$\left\{{}_{p-1}{}^{p}N^{(0)}\right\} = \left\{{}_{p-1}{}^{p-1}N\right\} - \sum_{r=1}^{4}\sum_{\rho=1}^{N_r}\left[1-\exp\left(-\frac{\Delta\zeta_r^p}{\lambda_{r\rho}}\right)\right]\left\{{}_{p-1}{}^{p-1}N_{r\rho}\right\} - \sum_{r=1}^{4}\left[Q_r^{\infty} + \sum_{\rho=1}^{N_r}\bar{S}_{r\rho}^{p}Q_{r\rho}\right]\left(\Delta\theta_T^p\left\{N_r^T\right\} + \Delta\theta_H^p\left\{N_r^H\right\}\right) \tag{55}$$

$$\left\{{}_{p-1}{}^{p}M^{(0)}\right\} = \left\{{}_{p-1}{}^{p-1}M\right\} - \sum_{r=1}^{4}\sum_{\rho=1}^{N_r}\left[1-\exp\left(-\frac{\Delta\zeta_r^p}{\lambda_{r\rho}}\right)\right]\left\{{}_{p-1}{}^{p-1}M_{r\rho}\right\} - \sum_{r=1}^{4}\left[Q_r^{\infty} + \sum_{\rho=1}^{N_r}\bar{S}_{r\rho}^{p}Q_{r\rho}\right]\left(\Delta\theta_T^p\left\{M_r^T\right\} + \Delta\theta_H^p\left\{M_r^H\right\}\right) \tag{56}$$

Note that Eqs. (55) and (56) result from setting the incremental displacements to zero in Eqs. (35) and (41), respectively. To be consistent in the evaluation of the tangent stiffness matrix for the first iteration, the $\{N\}$ corresponding to the geometric stiffness term [the last term in Eq. (54)] is taken simply as $\{{}_{p-1}{}^{p-1}N\}$. In all subsequent iterations $(n+1)$, the $\{N\}$ for the geometric stiffness term is taken as $\{{}_{p-1}{}^{p}N^{(n)}\}$. The incremental displacements are updated as follows:

$$\left\{U^{(n+1)}\right\} = \left\{U^{(n)}\right\} + \left\{\Delta U^{(n+1)}\right\} \tag{57}$$

The elemental force and force-couple resultants for $(n+1)\geq 1$ are updated using

$$\left\{{}_{p-1}{}^{p}N^{(n+1)}\right\} = \left\{{}_{p-1}{}^{p}N^{(0)}\right\} + [\tilde{A}^p]\left\{\Delta_{p-1}{}^{p}e^{(n+1)}\right\} + [\tilde{B}^p]\left\{\Delta_{p-1}{}^{p}\kappa^{(n+1)}\right\} \tag{58}$$

$$\left\{{}_{p-1}{}^{p}M^{(n+1)}\right\} = \left\{{}_{p-1}{}^{p}M^{(0)}\right\} + [\tilde{B}^p]\left\{\Delta_{p-1}{}^{p}e^{(n+1)}\right\} + [\tilde{D}^p]\left\{\Delta_{p-1}{}^{p}\kappa^{(n+1)}\right\} \tag{59}$$

where $\{\Delta_{p-1}{}^{p}e^{(n+1)}\}$ and $\{\Delta_{p-1}{}^{p}\kappa^{(n+1)}\}$, respectively, are the total incremental midplane in-plane strains and bending curvatures at iteration $(n+1)$.

The solution will be considered to be converged when

$$\frac{\left\|\left\{\Delta U_t^{(n+1)}\right\}\right\|_{\infty}}{\left\|\left\{U_t^{(n+1)}\right\}\right\|_{\infty}} < \text{tol}, \qquad \frac{\left\|\left\{\Delta U_r^{(n+1)}\right\}\right\|_{\infty}}{\left\|\left\{U_r^{(n+1)}\right\}\right\|_{\infty}} < \text{tol} \tag{60}$$

and/or

$$\left\|\left\{F_{\text{int}}^{(n)}\right\} - \left\{F_{\text{ext}}^{(n)}\right\}\right\|_2 < \text{tol} \tag{61}$$

where $\{U_t\}$ and $\{U_r\}$ refer to the translation and rotation components of the incremental global displacement vector, respectively, and tol is a suitable tolerance. Typically, the same tol is used in all three convergence measures. After convergence has been met, $\{N_{r\rho}\}$ and $\{M_{r\rho}\}$ are updated using Eqs. (45) and (46), respectively.

As previously mentioned, the iterations in a single time increment are performed using a total Lagrangian approach with all integrations carried out over the known configuration at t^{p-1}. Then after the incremental displacements have been converged, the reference

state is updated to the newly converged quasi-static equilibrium state at t^p with the updated global coordinates for node i given by

$$\begin{Bmatrix} X_i(t^p) \\ Y_i(t^p) \\ Z_i(t^p) \end{Bmatrix} = \begin{Bmatrix} X_i(t^{p-1}) \\ Y_i(t^{p-1}) \\ Z_i(t^{p-1}) \end{Bmatrix} + \begin{Bmatrix} u_i \\ v_i \\ w_i \end{Bmatrix} \tag{62}$$

Note that the TVATDKT-NL code can still be used for the static analysis of elastic structures under proportional loading by using t as the load proportionality factor. Because the TVATDKT-NL code is intended primarily for the analysis of viscoelastic structures where the load magnitudes are given as functions of the physical time t, the TVATDKT-NL code only uses load control, meaning that t must be increased from increment to increment. Hence, the TVATDKT-NL code is unable to trace the entire load-deflection behavior of elastic structures exhibiting snap through behavior. To accomplish this, a special method, such as the Riks method[50] or the modified Riks method (see Ref. 51), must be used. In both of these methods, the load parameter is allowed to vary within each increment and the additional equation needed to completely determine all of the unknowns at each iteration comes from an imposed equality constraint. In Riks method,[50] the constraint is placed on the arc length of the path followed in the load-deflection hyperspace, whereas in the modified Riks method (see Ref. 51), the square of the L2 norm of the incremental displacements is specified.

In general, finite rotations do not add vectorially (the final position of a body subjected to finite rotations about arbitrary axes depends on the order of the rotations).[52] Hence, in general, it is not accurate just to add the incremental rotations together to determine the total rotations, even though all of the rotations are represented in component form in the same stationary global coordinate system. Although techniques exist for the parameterization of large rotations,[52–54] they are not employed here because the total accumulated rotations are not needed in the updated Lagrangian approach that is used from increment to increment. However, because a total Lagrangian approach is used within each increment and the iterative changes in the rotations are added vectorially, the present formulation is limited to moderate values of incremental rotations. This simplifies the formulation somewhat, but at the cost of using more increments in determining the large-rotation response of structures. Given the wide availability of computational resources at the present time, this cost is not prohibitive.

Because no relevant terms have been neglected in the strain–displacement relations for thin shells, the present formulation is valid for thin shells undergoing small or large strains under the action of the applied loads, provided that the use of the constitutive law given in Eq. (20) is still valid and the incremental rotations are moderately small. For thick shells, transverse shear may be important and may need to be included in the formulation. Note that Eq. (20) corresponds to a linear relation between the PK2 stress tensor and the history of the Green–Saint-Venant strain tensor. It was found by Batra and Yu[55] that such a relationship may give qualitatively incorrect predictions for isotropic solids undergoing finite strains. Batra and Yu[55] showed that a linear relationship between the Cauchy stress tensor and the history of the relative Green–Saint-Venant strain tensor provided results that qualitatively agreed with experimental observations.

Numerical Examples

Several numerical examples are presented to demonstrate the accuracy of the TVATDKT-NL formulation and to present some key characteristics of the geometrically nonlinear response of viscoelastic structures. The first is a cantilever under a tip moment with two different time variations. Next, a ring under nonuniform external pressure is analyzed with the follower effects of the pressure load taken into account. Then, the creep buckling of a column under an axial load is examined. Following this, a composite cylindrical panel experiences snap through under a uniform deformation-dependent pressure load. In the final example, the thermal postbuckling of a composite plate is analyzed. Although the commercial code ABAQUS is used in validating some of the results, note that the current version of ABAQUS [ABAQUS/standard version 5.8 (Ref. 56)] is unable to handle the small or large deformations of viscoelastic composites.

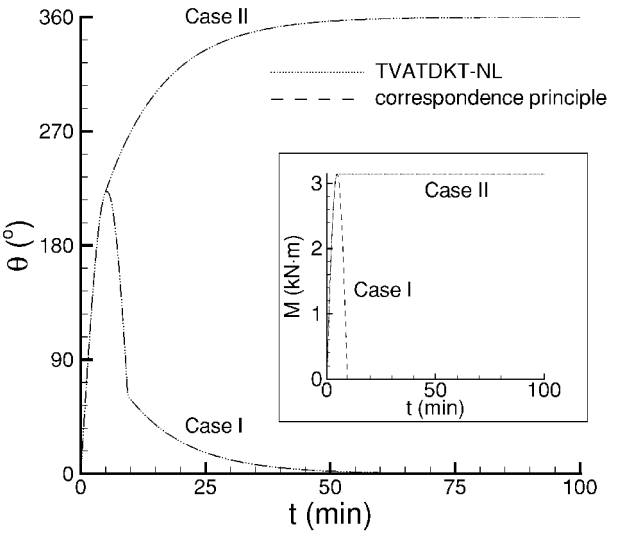

Fig. 2 Tip rotation of a linear viscoelastic cantilever subjected to a tip moment; inset shows time histories of applied tip moment.

Cantilever Under Tip Moment

The beam is 10.0 m long with a 1.0×0.1 m rectangular cross section. The relaxation modulus for the isotropic cantilever is taken to be

$$E(t) = E(0)[0.5 + 0.5\exp(-t/6)] \tag{63}$$

where t is in minutes. The initial modulus $E(0)$ is taken to be 1.2×10^8 Pa. To model the structure as a beam using a shell element that assumes a state of plane stress, Poisson's ratio is set to zero. This results in the bending stress being related to the bending strain history through $E(t)$.

Two time histories of tip moment with the following time variations are applied.

Case I:

$$M(t) = 1000\pi \sin(t/3)[1 - u(t - 3\pi)]\ \text{N} \cdot \text{m} \tag{64}$$

Case II:

$$M(t) = 1000\pi\{\sin(t/3)[1 - u(t - 1.5\pi)] + u(t - 1.5\pi)\}\text{N} \cdot \text{m} \tag{65}$$

where t is in minutes and $u(t)$ is the unit step function. The time histories of M for cases I and II are shown in an inset in Fig. 2.

The exact solution for this example can be developed as follows. For an elastic beam, the radius of curvature R is given by

$$1/R = \bar{M}/EI = v_{,xx} \Big/ \left[1 + (v_{,x})^2\right]^{\frac{3}{2}} \tag{66}$$

where $\bar{M}$ is the internal bending moment, E is the elastic modulus, I is the area moment of inertia, v is the transverse deflection, and subscript $,x$ represents $\mathrm{d}(\cdot)/\mathrm{d}x$. For a cantilever under a tip moment, the bending moment is constant throughout the beam and equal to the applied tip moment. Thus, the cantilever has a constant curvature. Also, in standard Euler–Bernoulli beam theory, the neutral axis does not exhibit strain. Hence, under any applied tip moment, the cantilever being studied here has a constant midplane length. This means that the angle θ subtended by the midplane of the elastic cantilever under tip moment M is given by

$$\theta = L/R = ML/EI \tag{67}$$

Equivalently, θ is the angle of rotation at the tip of the cantilever. The linear viscoelastic solution is developed using the correspondence principle,[40] which gives θ for the linear viscoelastic cantilever as

$$\theta = \mathcal{L}^{-1}\{\hat{M}L/s\hat{E}I\} \tag{68}$$

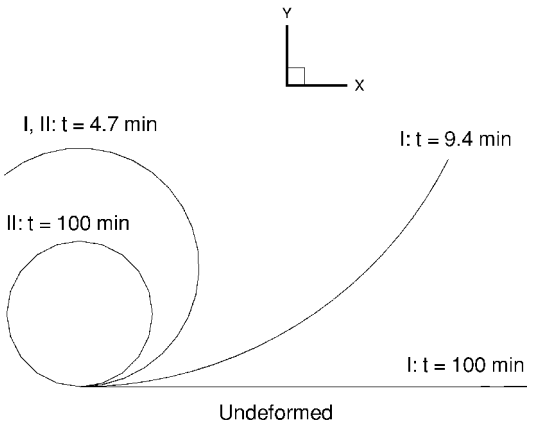

Fig. 3 Original and deformed TVATDKT-NL meshes at various times for a linear viscoelastic cantilever under two time variations of tip moment.

where $\mathcal{L}$ is the Laplace operator, $(\bar{\cdot})$ denotes the Laplace transform of $(\cdot)$, and s is the Laplace variable.

An exception to the rule that finite rotations do not add vectorially occurs when the axes of rotation are parallel.[52] Thus, the total rotation θ for this problem from the TVATDKT-NL analysis can be computed by simply adding the incremental rotation values together. Shown in Fig. 2 are the time histories of θ for cases I and II computed using 40 TVATDKT-NL elements and the correspondence principle. A time step of 0.1 min was used in marching the TVATDKT-NL finite element solution. Figure 3 shows a side view of the deflected meshes for both cases of applied tip moment at various times. For case I, the cantilever has nonzero deflection when the tip moment returns to zero at $t = 3\pi$ min because of the creep that has occurred under the applied load history. For case I at large t, the cantilever has essentially returned to its initial configuration. For case II after $t = 1.5\pi$ min, the applied tip moment is held constant at 1000π N · m. Hence, for large t in case II, the cantilever has deformed into a complete circle. The differences between the finite element and correspondence principle results cannot be distinguished.

Circular Ring Under External Pressure

The ring radius R is 6.0 in. (0.1524 m), whereas the width b and thickness h are 1.0 and 0.05 in. (0.0254 and 0.00127 m), respectively. The ring is composed of acetal resin (an engineering thermoplastic) with an initial elastic modulus $E(0) = 410{,}000$ psi (2.82681 GPa), which corresponds to a temperature of 73°F (22.78°C) (Ref. 57). Rogers and Lee[58] fit experimental creep data for the first 600 h presented by Warriner[57] to a creep compliance $\mathrm{D}(t)$ of

$$\frac{\mathrm{D}(t)}{\mathrm{D}(0)} = 1.0 + 0.00076t + 1.12\left[1 - \exp(-0.055t)\right] \tag{69}$$

where t is in hours. Hence, the creep compliance over the first 600 h is represented using a four-parameter fluid model. The corresponding relaxation modulus $E(t)$ can be found using Laplace transforms and was given by Yang and Lianis[17] to be

$$E(t)/E(0) = 0.46845\exp(-0.00035726t) + 0.53155\exp(-0.11700t) \tag{70}$$

The ring behaves as a curved beam and Poisson's ratio is set to zero for the finite element analyses.

The external pressure loading P on the ring at any given time t is of the form

$$P(\theta, t) = P_0(t)(1 - q\cos 2\theta) \tag{71}$$

where θ is as shown in Fig. 4 and always refers to the original configuration (body-attached pressure load). Results will be computed for several nonzero values of q.

Exploiting the symmetry about two planes in both the geometry and the loading, one-fourth of the ring is analyzed using either 40 TVATDKT-NL elements or 20 S4R elements of ABAQUS.[56] Element S4R is a four-node, doubly curved, quadrilateral shell element with six DOF per node. The following symmetry boundary conditions are used at points A and B which are indicated in Fig. 4.

Point A:

$$u = 0, \qquad \theta_y = \theta_z = 0 \tag{72}$$

Point B:

$$w = 0, \qquad \theta_x = \theta_y = 0 \tag{73}$$

where u, v, and w are the deflections in the x, y, and z directions; and θ_x, θ_y, and θ_z are the corresponding rotations about the x, y, and z axes. To prevent rigid-body motion in the y direction, v is restrained at point A. For all finite element analyses, the follower effects of the pressure load are taken into account.

The nondimensional load-deflection paths for the elastic case are shown in Fig. 5. Here the load parameter is taken as P_0, whereas the deflection is taken as w_A. The TVATDKT-NL and S4R results match very well. This elastic problem (including the follower effects of the pressure loading) was analyzed by Seide and Jamjoom[59] using numerical methods. As indicated in Ref. 59, bifurcation buckling

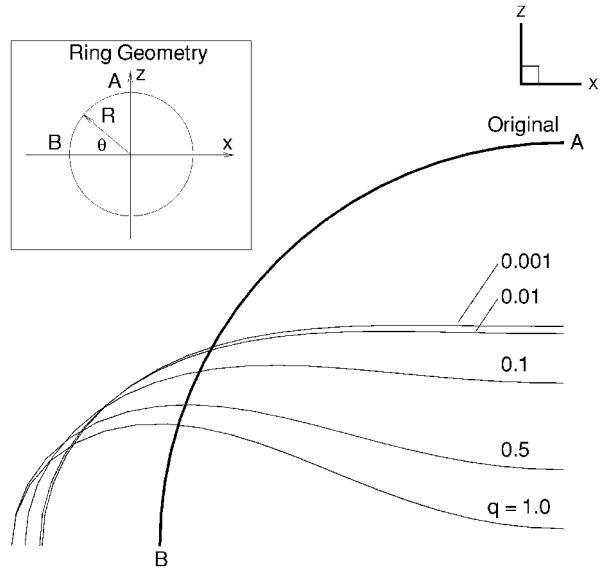

Fig. 4 Original and deformed shapes for an elastic ring under nonuniform pressure: deformed ring shapes computed using 40 TVATDKT-NL elements shown for nondimensional load level near $P_0bR^3/EI = 3.4$.

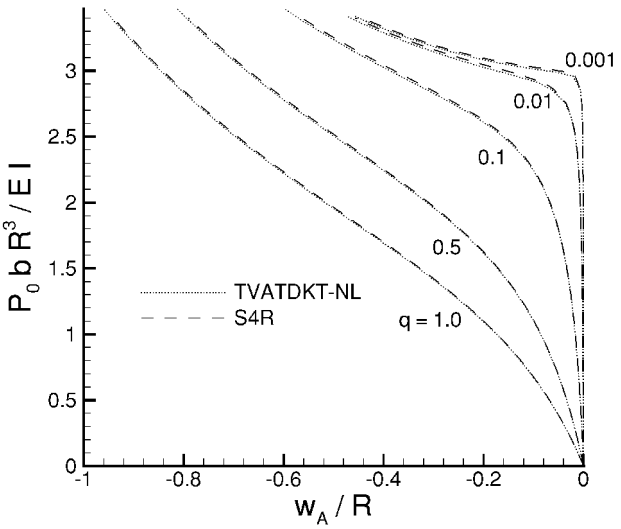

Fig. 5 Elastic load-deflection behavior of a ring under various nonuniform pressure loads $[P(\theta) = P_0(1 - q\cos 2\theta)]$.

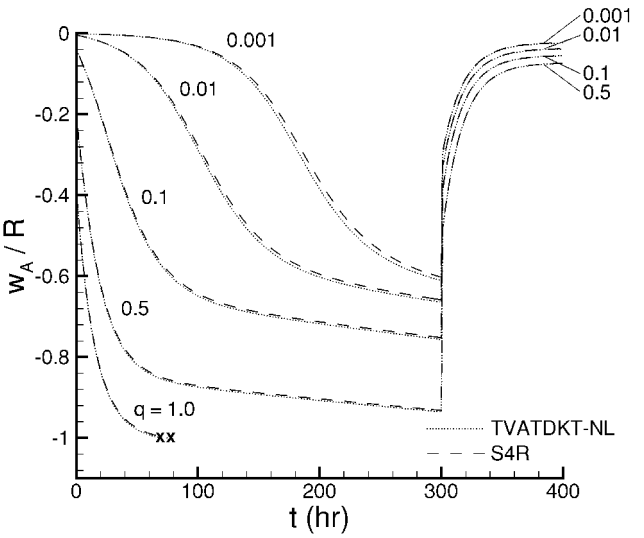

Fig. 6 Viscoelastic response of a ring under various nonuniform pressure loads.

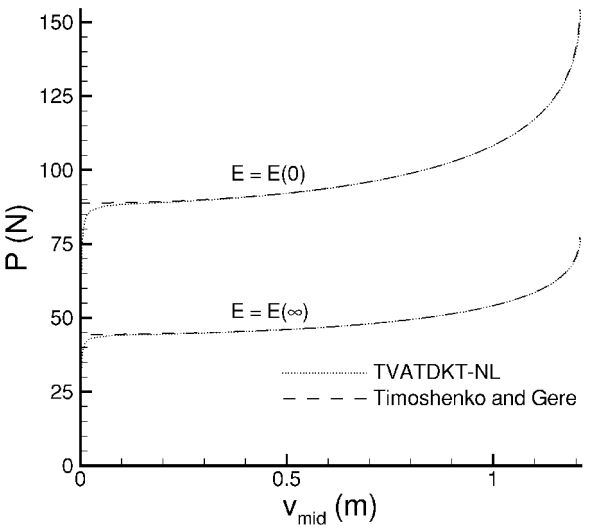

Fig. 7 Elastic load-deflection paths for a pinned–pinned column under axial load; TVATDKT-NL results computed using an initial imperfection amplitude of 7.5311×10^{-4} m; also elastica solutions of Timoshenko and Gere[60] for a geometrically perfect, inextensible structure.

occurs for the case of uniform pressure ($q = 0$) at a nondimensional load level of $P_0 bR^3/EI = 3.0$, where I is the area moment of inertia ($I = bh^3/12$). The effect of small nonzero q is to add a small imperfection in the loading so that a path very close to the bifurcation path is traced without the need for a bifurcation analysis to be performed. The original shape and the deformed elastic ring shapes near $P_0 bR^3/EI = 3.4$ for various values of q are shown in Fig. 4.

For viscoelastic analysis, the pressure magnitude $P_0(t)$ is ramped from zero to $\bar{P}_0$ over the first hour, then held constant for another 300 h, after which it is ramped back to zero over 1 h, and thereafter remains zero. A single value of $\bar{P}_0$, which is given as follows, is used:

$$\bar{P}_0 = 1.7[E(0)I/bR^3] \tag{74}$$

The viscoelastic results produced using the TVATDKT-NL and S4R elements are shown in Fig. 6. For the TVATDKT-NL finite element analysis, the time step size was 0.025 h during loading and unloading and 0.25 h during all other times. Reducing the time step by a factor of two and using 80 elements did not significantly change the TVATDKT-NL results for the case where $q = 0.001$. For this case, the deflection remains small for approximately the first 130 h, after which it increases at a substantially higher rate. Therefore, a delayed buckling due to creep is indicated, with the critical time for buckling estimated as 130 h. For the case where $q = 1.0$, the analysis was terminated when $w_A = -R$, which indicates that contact between point A and the point opposite to it has occurred. For the other cases, Fig. 6 indicates that the structure recovers a significant portion of its viscoelastic response during and after load removal.

Pinned–Pinned Column Under Axial Load

The column is 3.0 m long with a 0.3×0.03 m cross section. The relaxation modulus is the same as that used for the cantilever under a tip moment discussed earlier. The applied compressive axial load is P.

For elastic analysis, the stability of a perfect column is determined by examining the evolution of the lowest eigenvalue of the tangent stiffness matrix. Here, 40 TVATDKT-NL elements are used. The critical point using a Young's modulus $E = E(0)$ is determined as $P_{cr} = 88.9268$ N, which agrees well with the value of 88.8264 N computed using the classical Euler buckling load formula for a pinned–pinned column given by

$$P_{cr} = \pi^2(EI/L^2) \tag{75}$$

where I is the area moment of inertia and L is the column length. For an elastic column with $E = E(\infty)$, P_{cr} is determined to be 44.4634 and 44.4132 N from the finite element analysis and Eq. (75), respectively.

The elastic bifurcation problem can be studied without using any special bifurcation procedures incorporated in the TVATDKT-NL code by superimposing an initial imperfection onto the perfect structure. This imperfection is taken to be a small multiplicative constant times the eigenvector corresponding to the zero eigenvalue computed at the critical point of the perfect elastic structure using $E = E(0)$. It is well known that for a geometrically perfect, elastic pinned–pinned column, the first buckling mode is simply a half-sine wave, regardless of the value of E. The computed eigenvector shape agreed well with this. Shown in Fig. 7 are the load-deflection paths for the elastic case using both the initial and final values of the viscoelastic relaxation modulus. The imperfection is scaled to have a maximum magnitude of 7.5311×10^{-4} m. The column deflection is characterized by the midpoint transverse deflection v_{mid} for the load-deflection curves. Also shown in Fig. 7 are the results computed using the elastica solution of Timoshenko and Gere,[60] which assumes an inextensible perfect column. The present results with small initial imperfection approach those of Timoshenko and Gere,[60] as expected.

The stability of the viscoelastic column is determined by examining whether a small transverse deflection grows large or not with an axial load applied. Instability in such a case is commonly referred to as creep buckling. The small transverse deflection may either be introduced as an initial imperfection in the geometry or by applying a small sinusoidally varying distributed transverse load. For the present analysis, an initial imperfection is added to the column before the axial load is applied. This imperfection is once again taken to be a small factor times the lowest eigenvector computed at the critical point of the elastic analysis with $E = E(0)$.

The time histories of viscoelastic deflection are computed for a range of axial loads. In each case, the axial load is applied as a creep load at $t = 0$, that is, the load is applied suddenly at $t = 0$ and then held constant. However, for clarity only a few representative results are shown in Fig. 8. These results, computed using 40 TVATDKT-NL elements and a time step of 1.0 min, are taken to be converged because using 80 elements with a time step of 0.1 min did not significantly alter the results for $P = 50$ N. Although the axial load is applied as a creep load at $t = 0$ in each case, the time required to reach the final deformation state depends on the applied load level. This arises because the bending moment throughout the beam caused by the axial load is dependent on the transverse deflection of the beam. Furthermore, the transverse deformation depends on the applied loading and the initial imperfection. Hence, the internal bending moment in the column is time dependent. The final values of v_{mid} from the viscoelastic analyses match those computed using the long-term modulus value in the elastic analysis of the imperfect column.

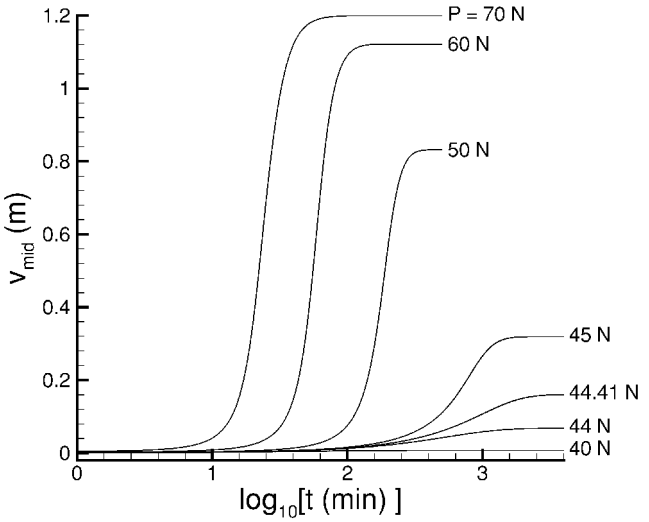

Fig. 8 Time histories of midpoint transverse deflection, v_{mid}, for various values of axial load P using an initial imperfection amplitude of 7.5311×10^{-4} m.

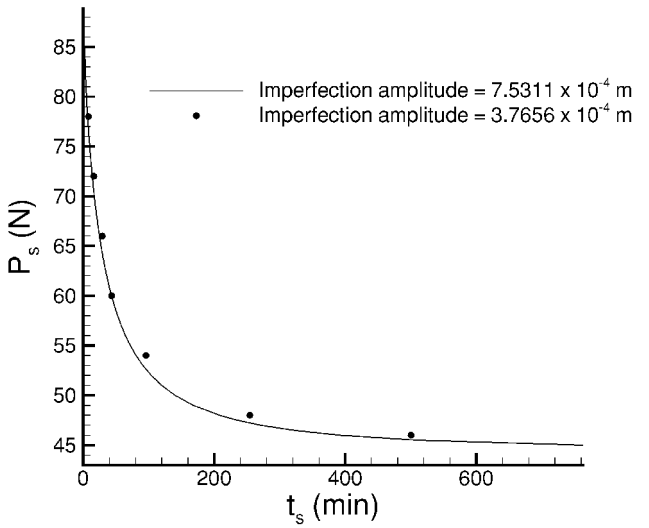

Fig. 9 Stability curves of a viscoelastic column for two levels of initial imperfection; t_s is the time required to reach $v_{min} = 0.2$ m under axial load P_s applied as a creep load at $t = 0$.

The creep buckling stability of the column can be characterized by v_{mid} remaining below a given level for a given loading and time duration. Either the loading or time duration of interest is selected, and then the safe time t_s or the safe load level P_s is determined. Here, for demonstrative purposes, the viscoelastic deformation will be taken to be acceptable if $v_{mid} < 0.2$ m. The time for v_{mid} to reach 0.2 m is plotted against the axial load in Fig. 9. Results are shown for two initial imperfection magnitudes. For an imperfection magnitude of 7.5311×10^{-4} m, the stability curve is computed using 40 data points, whereas only seven points are used for the 3.7646×10^{-4} m imperfection case. The two stability curves shown in Fig. 9 exhibit similar trends. Below an axial load of about 45 N, the structure remains safe for all times. For loads above this, the safe time t_s is determined by examining Fig. 9. Note that for loads slightly above the initial elastic buckling load, the viscoelastic column becomes unsafe nearly instantaneously. For relatively large loads, the critical time is not affected significantly by the magnitude of the initial imperfection. However, for loads approaching the final elastic buckling load from above, the safe time t_s computed for a given load P_s is significantly affected by the imperfection magnitude, because the stability curve there becomes horizontal in nature. On the other hand, the safe load P_s for a chosen time period t_s is affected less by the imperfection magnitude, even for loads approaching the final elastic buckling load level. The safe load level for which the viscoelastic deflections will remain safe for all time t for this well-behaved geometrically nonlinear example could have been determined by examining the elastic load-deflection paths computed using the final value of the viscoelastic relaxation modulus.

Cylindrical Panel Under Uniform Pressure

The length of the panel is 80.0 in. (2.032 m). The radius associated with the curvature of the panel is 100.0 in. (2.54 m), and the panel half-angle is 12 deg, corresponding to an arc length of 41.89 in. (1.064 m) for the two curved panel sides. The panel is taken to be supported on all edges by vertical diaphragms that are rigid in their own planes but perfectly flexible otherwise.

The composite panel is composed of four layers of GY70/339 graphite–epoxy with a symmetric cross-ply stacking sequence of $[0/90]_s$. Each layer is 0.08 in. (2.032×10^{-3} m) thick, which gives a total laminate thickness of 0.32 in. (8.128×10^{-3} m). The initial elastic properties are taken from Ref. 3 and are as follows:

$$E_1 = 42.0\,\text{Msi}\ (289.58\,\text{GPa}), \qquad G_{12}(0) = 0.6\,\text{Msi}\ (4.1368\,\text{GPa})$$

$$E_2(0) = 0.88\,\text{Msi}\ (6.0673\,\text{GPa}), \qquad \nu_{12} = 0.31 \tag{76}$$

Here E_1 is taken to be fiber dominated and, therefore, constant in time. The major Poisson's ratio ν_{12} is taken to be constant in computing the reduced stiffnesses Q_1–Q_4. By using these assumptions and also treating ν_{21} as constant in time, Q_1 will be constant in time. This is an acceptable approximation because Q_1 is fiber dominated. The viscoelastic time variation for the other three reduced stiffnesses is of the following form:

$$Q_r(t) = Q_r(0) f(t) \qquad \text{for } r = 2, 3, 4 \tag{77}$$

where

$$f(t) = f_0 + \sum_{i=1}^{10} f_i \exp\left(-\frac{t}{\lambda_i}\right) \tag{78}$$

The components of the normalized viscoelastic time variation $f(t)$ are given in Ref. 16. The panel is taken to be in a hygrothermal environment with a temperature of 151°F (66.11°C) and a moisture level of 0.1%. The horizontal shift factor corresponding to these environmental conditions is 10^{-4} as taken from Ref. 2. Furthermore, the panel is assumed to be free of hygrothermal strains in this environment.

Because of the cross-ply stacking sequence and the double symmetry in the geometry, boundary conditions, and loading, the panel response can be analyzed using one-fourth of the panel with proper symmetry conditions enforced on two edges. The deformation-dependent pressure loading of magnitude P_0 is applied pointing toward the center of curvature of the panel (external pressure). The load-deflection curve for the elastic case using the initial material properties given in Eq. (76) is shown in Fig. 10, where w_{mid} is the midpoint transverse deflection. The present results using 288 ATDKT-NL elements appear to agree fairly well with the results produced using 144 S4R elements. The mesh sizes are sufficient for accurate calculations because using either 512 ATDKT-NL or 256 S4R elements did not significantly change either set of results. Note that the modified Riks method (see Ref. 51) has been used with the ATDKT-NL and S4R analyses to trace the entire load-deflection path. Note that when the panel snaps, it does not snap to an inverted position because of the applied boundary conditions. Although snap through is truly a dynamic event, it has been inferred based on the static load-deflection behavior. The limit load is calculated to be 1.2942 psi (8.9231×10^3 Pa). Checks for possible bifurcation buckling are not included in the present analysis.

As shown in Fig. 10, the static elastic load-deflection can be partially traced using the TVATDKT-NL code, which uses load-control with the time t taken as the load-proportionality factor. Because the tangent stiffness matrix is singular at the limit point, the limit load cannot be both found exactly and bypassed in a single run using load control. To jump from a point just below the limit load to a stable static equilibrium point with higher load value, the incremental values of the load proportionality factor t must be chosen carefully.

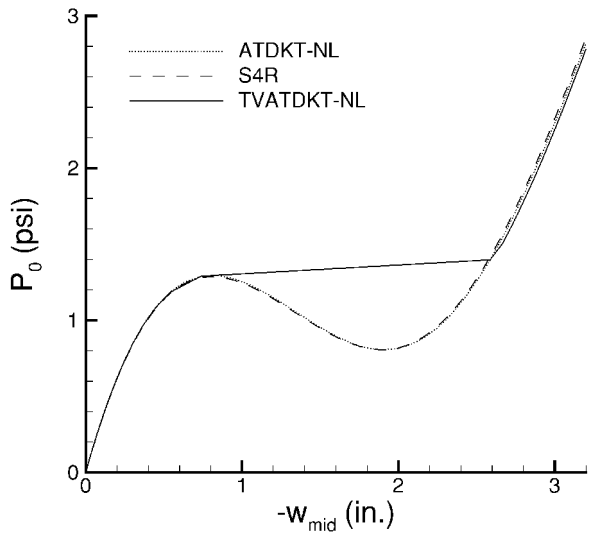

Fig. 10 Elastic load-deflection path (using the initial viscoelastic material properties) for a composite cylindrical panel under uniform pressure.

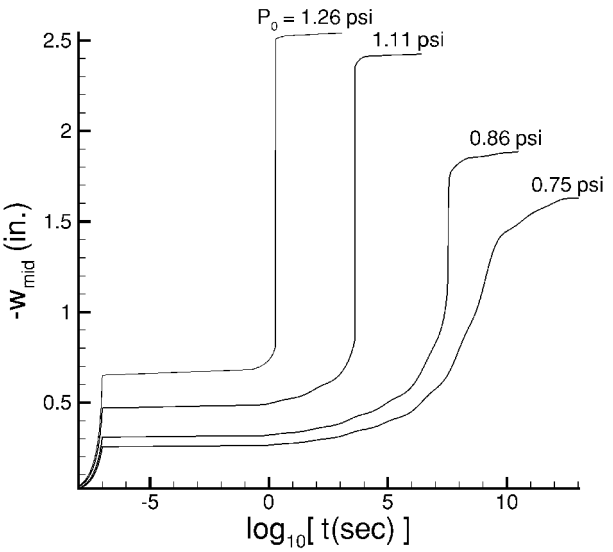

Fig. 11 Time histories of center point deflection for a viscoelastic composite cylindrical panel under various values of step pressure load.

This jump in the results using 288 TVATDKT-NL elements is indicated in Fig. 10 by the nearly horizontal line in the middle of the load-deflection curve.

For viscoelastic analysis, the applied pressure is ramped from 0 to P_0 over the first 10^{-7} s and held constant thereafter. A time step of $\Delta t = 10^{-8}$ s ($\Delta\zeta = 10^{-4}$ s) is used during load ramp-up. After ramp-up, the reduced time step increases as a geometric series as follows:

$$\Delta\zeta^p = \Delta\zeta^0 (r)^p \tag{79}$$

The time histories of viscoelastic center point deflection for various final magnitudes P_0 of applied pressure are shown in Fig. 11, using $\Delta\zeta^0 = 6000$ s ($\Delta t^0 = 0.6$ s) and $r = 1.08$ with 288 TVATDKT-NL elements. Using a time step approximately one order of magnitude smaller for all t ($r = 1.007$) did not significantly alter the viscoelastic results for $P_0 = 1.11$ psi (7.6531×10^3 Pa). For the cases exhibiting delayed snap through, the deflection magnitude increases at a finite rate until viscoelastic snap through occurs, which is indicated by a vertical tangent for the deflection vs time curve. Near viscoelastic snap through, the time step size is reduced in determining the snap through point. Once again, the critical point for snap through is not found exactly in the single-run results shown in Fig. 11 because

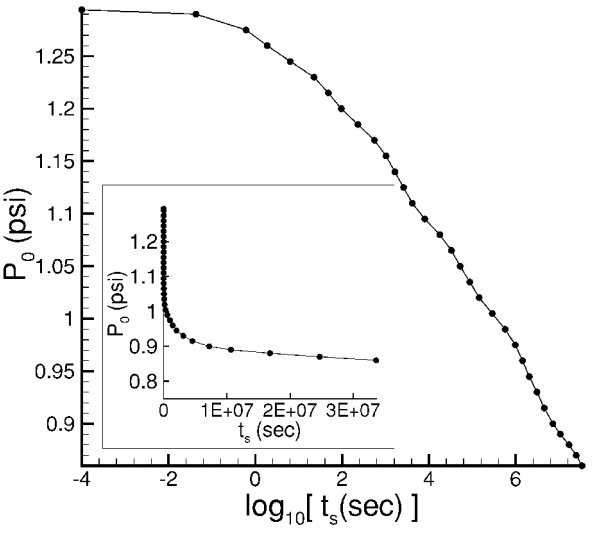

Fig. 12 Step pressure magnitude P_0 vs critical time t_s to viscoelastic snap through for a composite cylindrical panel.

the analysis is unable to converge right at the limit point, regardless of what size time step is used. After snap through, the viscoelastic deflection then continues to increase.

As can be observed from Fig. 11, the viscoelastic structure will exhibit snapping for a range of loads, if those loads are applied for a sufficiently long time. The lower limit on P_0 for which viscoelastic snap through will occur is found to be approximately 0.86 psi (5.92940×10^3 Pa). Note, that for P_0 values below this, the deflection may still grow to be relatively large, even though snap through does not occur. The time t_s, of snap through is plotted against P_0 in Fig. 12. For $P_0 \geq 1.2942$ psi (8.9231×10^3 Pa), the viscoelastic panel snaps at the instant the pressure magnitude reaches 1.2942 psi.

A check on the critical time computed for viscoelastic snap-through is performed using the quasi-elastic method.[39] Here, the quasi-elastic approximation for the viscoelastic deflection for a given time t^p is computed using a fictitious elastic reduced stiffness matrix $[\bar{Q}_E]$ equal to $[\bar{C}(\zeta^p)]^{-1}$, where $[\bar{C}(\zeta^p)]$ is the matrix of transformed reduced creep compliances. Note that $[\bar{Q}_E(\zeta^p)]$ is not exactly equal to $[\bar{Q}(\zeta^p)]$ because $[\bar{C}(\zeta)]$ and $[\bar{Q}(\zeta)]$ are not inverses of one another except for $\zeta = 0$ and ∞. Although the quasi-elastic method is more suited to situations where a closed-form solution exists, it can be implemented using a numerical technique, such as the finite element method. To use a quasi-elastic finite element approach to determine the time history of viscoelastic deformation, a separate finite element analysis must be performed for each discrete time considered. Also, note that in the case of nonlinear deformations where more than one quasi-elastic deformation state corresponds to a given load magnitude, the correct quasi-elastic deformation state can be determined from knowledge of the previous viscoelastic deformations.

Here, the applied pressure loading is ramped up over an extremely short time such that the pressure loading is applied essentially as a creep load at $t = 0$. For this nonlinear problem, the direction of the pressure loading changes as time evolves. However, this change is very gradual at all times except that corresponding to snap through. Hence, the computed critical time for viscoelastic snap through can be checked by determining the elastic load-deflection path with material properties corresponding to $[\bar{Q}_E(\zeta_s)]$, where ζ_s is the reduced time corresponding to t_s. The predicted elastic limit load should then match the applied creep load magnitude used in the viscoelastic analysis.

Shown in Fig. 13 are the elastic load-deflection curves corresponding to several values of t_s. Horizontal lines corresponding to the pressure magnitudes P_0 causing viscoelastic snap through at $t = t_s$ are also shown. The computed elastic limit loads are in good agreement with the applied loads used in the viscoelastic analysis, indicating that the predicted times t_s for the viscoelastic analyses are accurate. Note that the severity of the snap through decreases as t_s increases, until a snap through is no longer indicated. This decrease

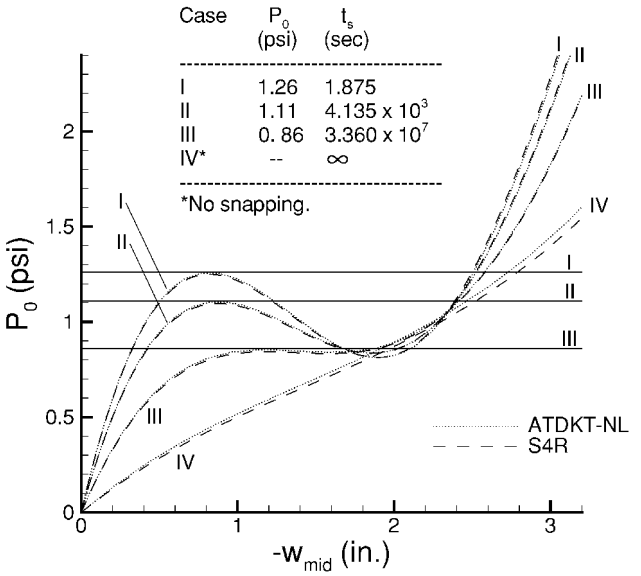

Fig. 13 Elastic load-deflection paths using creep compliance properties corresponding to time t_s: horizontal lines correspond to the load levels P_0 necessary to cause snapping at t_s as predicted by the viscoelastic TVATDKT-NL analyses.

in snap through severity is also indicated in Fig. 11. For extremely large times, the agreement between the ATDKT-NL and S4R elastic load-deflection curves decreases, likely because of the growing importance of transverse shear effects, which are included in the S4R formulation but not in the ATDKT-NL formulation. Hence, the TVATDKT-NL formulation (which reduces to the ATDKT-NL formulation in the elastic case) is likely to be slightly in error for extremely large times.

Although not presented here, similar types of viscoelastic results were obtained for an isotropic hinged cylindrical panel undergoing snap through under the action of a centrally applied point force.[61] For that example, the TVATDKT-NL viscoelastic results were found to be in good agreement with viscoelastic results produced using element S4R of ABAQUS.[56]

Thermal Postbuckling of an Antisymmetric Angle-Ply Plate

The plate is square with a side length L equal to 50 in. (1.27 m). The plate edges are parallel to the global x and y directions. The pinned boundary conditions are as follows:

$$x = 0,\ L: \quad u = w = 0 \qquad \text{and} \qquad M_x = N_{xy} = 0$$
$$y = 0,\ L: \quad v = w = 0 \qquad \text{and} \qquad M_y = N_{xy} = 0 \tag{80}$$

The plate has an antisymmetric stacking sequence of $[\pm 45]_a$. Each of the four layers has a thickness of 0.05 in. (1.27×10^{-3} m), which gives a total laminate thickness of 0.2 in. (5.08×10^{-3} m).

The plate is composed of T300/934 graphite–epoxy with the following viscoelastic material properties at $t = 0$ taken from Flaggs and Crossman[3]:

$$E_1 = 21 \text{ Msi } (144.79 \text{ GPa}), \qquad E_2 = 1.5 \text{ Msi } (10.342 \text{ GPa})$$
$$\alpha_1 = 0.05 \times 10^{-6}/°\text{F } (9 \times 10^{-8}/°\text{C})$$
$$G_{12} = 0.7 \text{ Msi } (4.8263 \text{ GPa}), \qquad \nu_{12} = 0.29$$
$$\alpha_2 = 16.5 \times 10^{-6}/°\text{F } (2.97 \times 10^{-5}/°\text{C}) \tag{81}$$

Because Q_1 is taken to be fiber-dominated, it will be treated as constant in time. The other three Q_r have the same normalized viscoelastic time variation and are given by

$$Q_r(t) = Q_r(0) f(t) = Q_r(0) \left[f_0 + \sum_{i=1}^{N} f_i \exp\left(-\frac{t}{\lambda_i} \right) \right] \quad \text{for } r = 2, 3, 4 \tag{82}$$

Table 1 Prony series coefficients and time constants for T300/934 graphite–epoxy

i	f_i	λ_i, s
0	1.78398×10^{-1}	——
1	4.96164×10^{-2}	5.21100×10^{2}
2	4.91345×10^{-2}	2.06800×10^{4}
3	5.29998×10^{-2}	1.07785×10^{6}
4	5.21760×10^{-2}	2.32300×10^{7}
5	8.50296×10^{-2}	1.67441×10^{9}
6	5.97267×10^{-2}	3.24064×10^{10}
7	1.56990×10^{-1}	1.69677×10^{12}
8	9.69593×10^{-2}	5.14749×10^{13}
9	2.18970×10^{-1}	1.49240×10^{15}

Table 2 Horizontal shift factors for T300/934 graphite–epoxy in an environment with 0.14% moisture

T, °F	T, °C	$\log_{10}[A_{TH}]$
77	25	0
122	50	−2.1176
167	75	−4.5647
212	100	−6.3529
257	125	−8.2353
302	150	−10.0706
347	175	−12

Using ABAQUS,[56] a nine-term ($N = 9$) Prony series is fit to experimental data for T300/934 presented by Crossman et al.[2] The Prony series components are given in Table 1. The plate is assumed to be free of hygrothermal strains in an environment with 0.14% moisture. The viscoelastic matrix is assumed to be hygrothermorheologically simple. The horizontal shift factor A_r is taken to be the same for Q_2–Q_4 and is subsequently denoted by A_{TH}. The values for $\log_{10}[A_{TH}]$ taken from Crossman et al.[2] are presented in Table 2. The horizontal shift factors for intermediate temperatures are determined using a linear interpolation for $\log_{10}[A_{TH}]$.

The viscoelastic plate is subjected to a range of thermal loads. In each case, the plate is initially free of thermal strains at a temperature T_i of 77°F (25°C). The temperature is ramped up using a linear variation from 77°F to its final temperature T_f over the first 10^{-7} s and then held constant. Hence, the thermal load $\Delta T = T_f - T_i$ is applied almost instantaneously. Here, only integer values of ΔT are considered. During ramp-up, the time step Δt is chosen to be $10^{-7}/\Delta T$, giving an increase of 1°F (5/9°C) in each increment. During this period, the change in reduced time ζ is determined as[56]

$$\Delta\zeta^p = \left(\left\{ \left[1 \Big/ A_{TH}(T^p) \right] - \left[1 \Big/ A_{TH}(T^{p-1}) \right] \right\} \Big/ \left(\ln A_{TH}(T^{p-1}) - \ln A_{TH}(T^p) \right) \right) \Delta t^p \tag{83}$$

After ramp-up, the time step size is chosen to be

$$\Delta t^p = 100\,(r)^p\, A_{TH}(T_f) \text{ s} \tag{84}$$

where r is the time step size ratio between consecutive increments.

A geometrically perfect, elastic, antisymmetric angle-ply plate with the boundary conditions given in Eq. (80) undergoes zero deformation under a uniform thermal load until the bifurcation point for thermal buckling is reached.[62,63] The elastic load-deflection path is determined by first finding the bifurcation point that corresponds to a singular tangent stiffness matrix. Next, the eigenvector corresponding to the zero eigenvalue is determined. A small constant times this eigenvector is then introduced as an initial imperfection in the plate geometry, and the analysis is started over. The viscoelastic plates are also analyzed using this initial imperfection.

An approximate viscoelastic solution can be determined using the quasi-elastic approach described by Schapery.[39] Both the quasi-elastic and viscoelastic results are computed using a uniform mesh of 512 TVATDKT-NL elements. For the viscoelastic analysis, $r = 1.08$ is used in Eq. (84) to determine the time step. Using a finer mesh

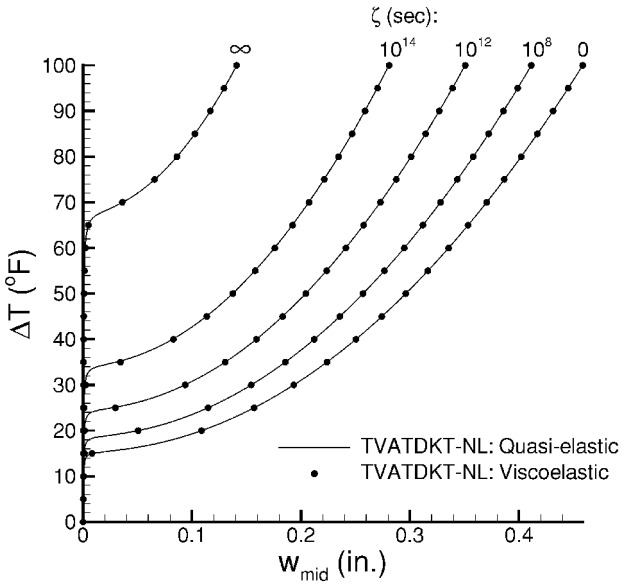

Fig. 14 Thin viscoelastic $[\pm 45]_a$ plate under uniform thermal load applied nearly instantaneously at $t = 0$ and then held constant; small initial imperfection is used in both the quasi-elastic and viscoelastic analyses ($\Delta T = T_f - T_i$ and $T_i = 77°F$).

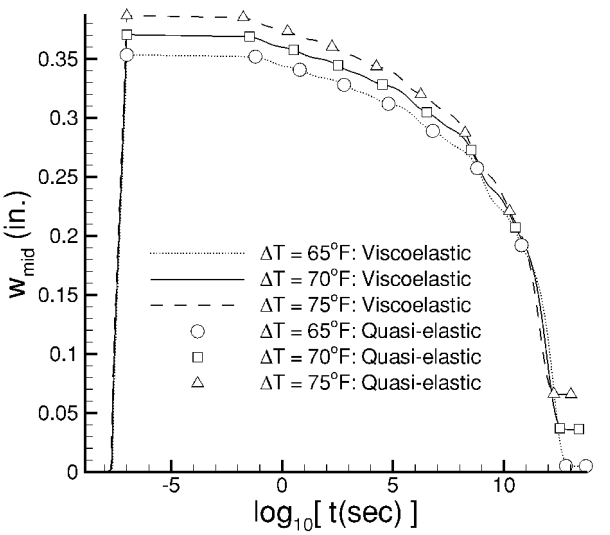

Fig. 15 Time history of viscoelastic midpoint transverse deflection of thin antisymmetric panel under various values of thermal load computed using viscoelastic and quasi-elastic TVATDKT-NL analyses; small initial imperfection is used in both the quasi-elastic and viscoelastic analyses ($\Delta T = T_f - T_i$ and $T_i = 77°F$).

of 1152 elements and a time step approximately one order of magnitude smaller for all t ($r = 1.007$) did not significantly change the viscoelastic results for $\Delta T = 100°F$ (37.78°C).

Shown in Fig. 14 are the quasi-elastic load-deflection paths using elastic properties corresponding to the viscoelastic relaxation moduli at various values of reduced times. Here w_{mid} denotes the transverse deflection at the plate center. Results computed at other values of reduced time are not shown for clarity in Fig. 14. In each case, the critical buckling mode consisted of a single half-sine wave in the x and y directions. The initial imperfection used in each case has a maximum magnitude of 2.48877×10^{-4} in. (6.3215×10^{-6} m). Also shown in Fig. 14 are the load-deflection pairs computed using viscoelastic finite element analysis. Note that $\zeta = 0$ viscoelastic results are actually the viscoelastic results after load ramp-up, that is, the ζ for the initial viscoelastic results is not exactly zero, but still relatively very small. Also, the $\zeta = \infty$ viscoelastic results are actually near-equilibrium results computed at reduced times less than infinity. The mode shape of viscoelastic deformation for each value of ΔT considered remained a single half-sine wave in the x and y directions for all times. Note that Fig. 14 does not show how the viscoelastic deformation would vary with changes in ΔT applied at a given time. Rather, for the viscoelastic case, the curves shown in Fig. 14 can be used together to determine how the viscoelastic deformation varies with time for a range of load levels, where the thermal load in each case is applied nearly instantaneously at $t = 0$ and then held constant. Also, recall that the physical time t corresponding to a given reduced time ζ depends on the temperature history.

The bifurcation temperature is observed to increase as larger times are used in the quasi-elastic analysis. This counterintuitive result is explained by noting that the compressive forces caused by the thermal load decrease because of viscoelastic relaxation, which is reflected in the quasi-elastic analysis by the use of degraded Q_2–Q_4 properties. In each quasi-elastic case, the bifurcation temperature computed using the TVATDKT-NL code agreed well with that computed using the formula neglecting transverse shear effects presented by Tauchert.[63] The bifurcation temperature at $t = 0$ computed using both Tauchert's closed-form solution[63] and the finite element code is 15.42°F (−9.21°C), whereas the final bifurcation temperature is computed to be 68.07°F (20.04°C) and 68.09°F (20.05°C) from the closed-form solution[63] and the TVATDKT-NL analysis, respectively.

The time histories of deformation computed using the viscoelastic and quasi-elastic finite element analyses are shown in Fig. 15 for several values of thermal load. The decrease in viscoelastic deformation as time evolves is also explained by the relaxation of the compressive force resultants caused by the imposed thermal strains and boundary conditions. Note that as T_f increases in magnitude, the time to reach the long-term equilibrium state decreases. This occurs because of the speed-up of the viscoelastic response with increasing T_f as incorporated through the hygrothermorheologically simple postulate made for the matrix material. By examining Fig. 14, it should be apparent that if the viscoelastic deflections for various values of ΔT were plotted vs reduced time ζ as opposed to physical time t in Fig. 15, the various deflection curves would not cross over each other as shown in Fig. 15. From Figs. 14 and 15, it is clear that for thermal loads below the final critical ΔT value of 68.09°F, the final viscoelastic deformation is essentially zero. The agreement between the quasi-elastic and viscoelastic results appears to be very good, because the stress resultants and deformations change slowly with time and a single mode of viscoelastic deformation occurs for this well-behaved, geometrically nonlinear example.

Summary

A thin shell element for the large-deformation analysis of linear viscoelastic laminated composites has been presented. The triangular flat shell element is obtained as the superposition of the DKT plate bending element and a membrane element having the same nodal DOF as the AT, which result in six DOF at each corner node and a total of 18 DOF for the element. The material is modeled as being hygrothermorheologically simple. Exponential series are used to represent the linear viscoelastic relaxation moduli. The incremental stresses over a time step are divided into parts corresponding to the incremental strains and the viscoelastic memory loads. These memory loads are updated at the end of an increment using recursion relations involving the preceding memory load values and terms corresponding to the incremental strains that were just converged. The viscoelastic tangent stiffness matrix is similar to that occurring in the elastic case, but with the usual $[A;\ B;\ D]$ matrices replaced by matrices that account for the relaxation over the current time step of the portion of the stresses caused by the current incremental strains.

The large deformations and stability of linear elastic and viscoelastic structures were examined. Examples were presented where viscoelastic buckling or snap through was observed to occur at a range of critical times for a range of applied load magnitudes. The critical time to buckling or snap through increased as the magnitude of the applied load decreased. For situations where a geometrically perfect elastic structure would undergo bifurcation buckling with no prebuckling deformation, it was necessary to add either an

imperfection in the loading or geometry to study the stability of a similar viscoelastic structure using a full viscoelastic analysis. The critical time for instability of viscoelastic structures is, of course, affected by the size of the imperfection. Hence, for the analysis of nonacademic problems, the imposed imperfection must be chosen carefully, based on the expected imperfections that would occur in the geometry and loading of the actual structure.

The quasi-elastic approach provides a convenient way to assess the accuracy of a full viscoelastic analysis when other results (analytical, numerical, or experimental) are unavailable. Although not shown here, it is well known that the quasi-elastic method provides sufficient accuracy only in situations where the viscoelastic relaxation moduli (or creep compliances), the stress resultants, and the deformations all vary slowly with time. Note that to determine the deflection history of complex viscoelastic structures, a numerical approach, such as the finite element method, must be used. However, for finite element analysis, it is more cumbersome to use a quasi-elastic approach than a full viscoelastic approach to determine the complete time history of viscoelastic deflection, especially in the case of large deformations.

Acknowledgments

Daniel C. Hammerand was supported during this research by a National Science Foundation Graduate Research Fellowship. The support for Rakesh K. Kapania during this research was provided by Grant DAAH04-95-1-0175 from the Army Research Office with Gary Anderson as the Grant Monitor and is greatly appreciated. Sandia is a multiprogram laboratory operated by Sandia Corporation, a Lockheed Martin Company, for the U.S. Department of Energy under Contract DE-AC04-94AL85000. We would like to thank Bernard Grossman, Department Head, Aerospace and Ocean Engineering, and Eugene Cliff, Associate Director, Interdisciplinary Center for Applied Mathematics, for providing considerable computational resources. We would also like to thank Raymond Plaut (Department of Civil Engineering), P. Mohan (former Department of Aerospace and Ocean Engineering graduate student) and Jing Li (Department of Aerospace and Ocean Engineering) for valuable discussions held during the course of this research.

References

[1]Aklonis, J. J., and MacKnight, W. J., *Introduction to Polymer Viscoelasticity*, 2nd ed., Wiley, New York, 1983.

[2]Crossman, F. W., Mauri, R. E., and Warren, W. J., "Moisture-Altered Viscoelastic Response of Graphite/Epoxy Composites," *Advanced Composite Materials—Environmental Effects*, STP 658, American Society for Testing and Materials, Philadelphia, 1978, pp. 205–220.

[3]Flaggs, D. L., and Crossman, F. W., "Analysis of the Viscoelastic Response of Composite Laminates During Hygrothermal Exposure," *Journal of Composite Materials*, Vol. 15, Jan. 1981, pp. 21–40.

[4]White, J. L., "Finite Elements in Linear Viscoelasticity," *Proceedings of 2nd Conference on Matrix Methods in Structural Mechanics*, U.S. Air Force Flight Dynamics Lab., AFFDL-TR-68-150, Wright–Patterson AFB, OH, 1968, pp. 489–516.

[5]Taylor, R. L., Pister, K. S., and Goudreau, G. L., "Thermomechanical Analysis of Viscoelastic Solids," *International Journal for Numerical Methods in Engineering*, Vol. 2, No. 1, 1970, pp. 45–59.

[6]Wang, Y. Z., and Tsai, T. J., "Static and Dynamic Analysis of a Viscoelastic Plate by the Finite Element Method," *Applied Acoustics*, Vol. 25, No. 2, 1988, pp. 77–94.

[7]Ben-Zvi, R., "A Simple Implementation of a 3D Thermo-Viscoelastic Model in a Finite Element Program," *Computers and Structures*, Vol. 34, No. 6, 1990, pp. 881–883.

[8]Krishna, A., Harper, B. D., and Lee, J. K., "Finite Element Viscoelastic Analysis of Temperature and Moisture Effects in Electronic Packaging," *Journal of Electronic Packaging*, Vol. 117, No. 3, 1995, pp. 192–200.

[9]Lin, K. Y., and Hwang, I. H., "Thermo-Viscoelastic Response of Graphite/Epoxy Composites," *Journal of Engineering Materials and Technology*, Vol. 110, No. 2, 1988, pp. 113–116.

[10]Lin, K. Y., and Hwang, I. H., "Thermo-Viscoelastic Analysis of Composite Materials," *Journal of Composite Materials*, Vol. 23, June 1989, pp. 554–569.

[11]Hilton, H., and Yi, S., "Dynamic Finite Element Analysis of Viscoelastically Damped Composite Structures," *Applications of Supercomputers in Engineering II*, edited by C. A. Brebbia, D. Howard, and A. Peters, Elsevier Applied Science, London, 1991, pp. 495–511.

[12]Yi, S., and Hilton, H., "Dynamic Finite Element Analysis of Viscoelastic Composite Plates in the Time Domain," *International Journal for Numerical Methods in Engineering*, Vol. 37, No. 23, 1994, pp. 4081–4096.

[13]Yi, S., Ahmad, M. F., and Ramesh, A., "Data Parallel Computation for Thermo-Viscoelastic Analysis of Composite Structures," *Advances in Engineering Software*, Vol. 27, No. 1–2, 1996, pp. 97–102.

[14]Lin, K. Y., and Yi, S., "Analysis of Interlaminar Stresses in Viscoelastic Composites," *International Journal of Solids and Structures*, Vol. 27, No. 7, 1991, pp. 929–945.

[15]Yi, S., and Hilton, H., "Hygrothermal Effects on Viscoelastic Responses of Laminated Composites," *Composites Engineering*, Vol. 5, No. 2, 1995, pp. 183–193.

[16]Hammerand, D. C., and Kapania, R. K., "Thermoviscoelastic Analysis of Composite Structures Using a Triangular Flat Shell Element," *AIAA Journal*, Vol. 37, No. 2, 1999, pp. 238–247.

[17]Yang, T. Y., and Lianis, G., "Large Displacement Analysis of Viscoelastic Beams and Frames by the Finite Element Method," *Journal of Applied Mechanics*, Vol. 41, No. 3, 1974, pp. 635–640.

[18]Key, S. W., "A Finite Element Procedure for the Large Deformation Dynamic Response of Axisymmetric Solids," *Computer Methods in Applied Mechanics and Engineering*, Vol. 4, No. 2, 1974, pp. 195–218.

[19]Shen, Y. P., Zheng, J. S., and Zhou, Z., "Dynamic Incremental Constitutive Relation and Dynamic Response of Viscoelastic Solid," *Computational Mechanics: Proceedings of the Asian Pacific Conference on Computational Mechanics*, edited by Y. K. Cheung, J. H. W. Lee, and A. Y. T. Leung, Rotterdam, Brookfield, VT, 1991, pp. 639–644.

[20]Shen, Y. P., Hasebe, N., and Lee, L. X., "The Finite Element Method of Three-Dimensional Nonlinear Viscoelastic Large Deformation Problems," *Computers and Structures*, Vol. 55, No. 4, 1995, pp. 659–666.

[21]Roy, S., and Reddy, J. N., "Nonlinear Viscoelastic Finite Element Analysis of Adhesive Joints," *Tire Science and Technology*, Vol. 16, No. 3, 1988, pp. 146–170.

[22]Jenkins, C., and Leonard, J. W., "Transient Non-Linear Deformation of Viscoelastic Membrane Structures," *Structural Engineering Review*, Vol. 3, 1991, pp. 197–204.

[23]Faria, L. O., Oden, J. T., Yavari, B., Tworzydlo, W. W., Bass, J. M., and Becker, E. B., "Tire Modeling by Finite Elements," *Tire Science and Technology*, Vol. 20, No. 1, 1992, pp. 33–56.

[24]Padovan, J., "Finite Element Analysis of Steady and Transiently Moving/Rolling Nonlinear Viscoelastic Structure—I. Theory," *Computers and Structures*, Vol. 27, No. 2, 1987, pp. 249–257.

[25]Kennedy, R., and Padovan, J., "Finite Element Analysis of Steady and Transiently Moving/Rolling Nonlinear Viscoelastic Structure—II. Shell and Three-Dimensional Simulations," *Computers and Structures*, Vol. 27, No. 2, 1987, pp. 259–273.

[26]Nakajima, Y., and Padovan, J., "Finite Element Analysis of Steady and Transiently Moving/Rolling Nonlinear Viscoelastic Structure—III. Impact/Contact Simulations," *Computers and Structures*, Vol. 27, No. 2, 1987, pp. 275–286.

[27]Marques, S. P. C., and Creus, G. J., "Geometrically Nonlinear Finite Element Analysis of Viscoelastic Composite Materials Under Mechanical and Hygrothermal Loads," *Computers and Structures*, Vol. 53, No. 2, 1994, pp. 449–456.

[28]Wilson, D. W., and Vinson, J. R., "Viscoelastic Analysis of Laminated Plate Buckling," *AIAA Journal*, Vol. 22, No. 7, 1984, pp. 982–988.

[29]Wilson, D. W., and Vinson, J. R., "Viscoelastic Buckling Analysis of Laminated Composite Columns," *Recent Advances in Composites in the United States and Japan*, edited by J. R. Vinson and M. Taya, STP 864, American Society for Testing and Materials, Philadelphia, 1985, pp. 368–383.

[30]Vinogradov, A. M., "Creep Buckling of Asymmetric Laminated Beam Columns," *Compression Response of Composite Structures*, edited by S.E. Groves and A.L. Highsmith, STP 1185, American Society for Testing and Materials, Philadelphia, 1994, pp. 55–64.

[31]Kim, C. G., and Hong, C. S., "Viscoelastic Sandwich Plates with Crossply Faces," *Journal of Structural Engineering*, Vol. 114, No. 1, 1988, pp. 150–164.

[32]Huang, N. N., "Viscoelastic Analysis of von Karman Laminated Plates Under In-Plane Compression with Initial Deflection," *International Journal of Non-Linear Mechanics*, Vol. 32, No. 6, 1997, pp. 1065–1075.

[33]Huang, N. N., "Creep Deflection of Viscoelastic Laminated Cylindrical Panels with Initial Deflection Under Axial Compression," *Composites: Part B*, Vol. 30, No. 2, 1999, pp. 145–156.

[34]Touati, D., and Cederbaum, G., "Postbuckling of Non-Linear Viscoelastic Imperfect Laminated Plates. Part II: Structural Analysis," *Composite Structures*, Vol. 42, No. 1, 1998, pp. 43–51.

[35]Shalev, D., and Aboudi, J., "Postbuckling Analysis of Viscoelastic Laminated Plates Using Higher-Order Theory," *International Journal of Solids and Structures*, Vol. 27, No. 14, 1991, pp. 1747–1755.

[36]Bathe, K. J., *Finite Element Procedures*, Prentice–Hall, Englewood Cliffs, NJ, 1996, pp. 515, 522–528.

[37]Schapery, R. A., "On the Characterization of Nonlinear Viscoelastic Materials," *Polymer Engineering and Science*, Vol. 9, No. 4, 1969, pp. 295–310.

[38]Jones, R. M., *Mechanics of Composite Materials*, 1st ed., Hemisphere, New York, 1975, pp. 114–120.

[39]Schapery, R. A., "A Method of Viscoelastic Stress Analysis Using Elastic Solutions," *Journal of the Franklin Institute*, Vol. 279, No. 4, 1965, pp. 268–289.

[40]Christensen, R. M., *Theory of Viscoelasticity, An Introduction*, 2nd ed., Academic, New York, 1982, pp. 45, 46.

[41]Mohan, P., and Kapania, R. K., "Updated Lagrangian Formulation of a Flat Triangular Element for Thin Laminated Shells," *AIAA Journal*, Vol. 36, No. 2, 1998, pp. 273–281.

[42]Batoz, J. L., Bathe, K. J., and Ho, L. W., "A Study of Three-Node Triangular Plate Bending Elements," *International Journal for Numerical Methods in Engineering*, Vol. 15, No. 12, 1980, pp. 1771–1812.

[43]Allman, D. J., "A Compatible Triangular Element Including Vertex Rotations for Plane Elasticity Analysis," *Computers and Structures*, Vol. 19, No. 1-2, 1984, pp. 1–8.

[44]Ertas, A., Krafcik, J. T., and Ekwaro-Osire, S., "Performance of an Anisotropic Allman/DKT 3-Node Thin Triangular Flat Shell Element," *Composites Engineering*, Vol. 2, No. 4, 1992, pp. 269–280.

[45]Cook, R. D., "On the Allman Triangle and a Related Quadrilateral Element," *Computers and Structures*, Vol. 22, No. 6, 1986, pp. 1065–1067.

[46]Kapania, R. K., and Mohan, P., "Static, Free Vibration and Thermal Analysis of Composite Plates and Shells Using a Flat Triangular Shell Element," *Computational Mechanics*, Vol. 17, No. 5, 1996, pp. 343–357.

[47]Mohan, P., and Kapania, R. K., "Analysis of General Shells Under Deformation Dependent Pressure Loads Using a Flat Triangular Shell Element," *Proceedings of the 39th AIAA/ASME/ASCE/AHS/ASC Structures, Structural Dynamics and Materials Conference*, AIAA, Reston, VA, 1998, pp. 534–541.

[48]Fafard, M., and Dhatt, G., and Batoz, J. L., "A New Discrete Kirchhoff Plate/Shell Element with Updated Procedures," *Computers and Structures*, Vol. 31, No. 4, 1989, pp. 591–606.

[49]Yang, T. Y., *Finite Element Structural Analysis*, Prentice–Hall, Englewood Cliffs, NJ, 1986, Chap. 11, p. 354.

[50]Riks, E., "An Incremental Approach to the Solution of Snapping and Buckling Problems," *International Journal of Solids and Structures*, Vol. 15, No. 7, 1979, pp. 529–551.

[51]Crisfield, M. A., "A Fast Incremental/Iterative Solution Procedure that Handles Snap-Through," *Computers and Structures*, Vol. 13, No. 1–3, 1981, pp. 55–62.

[52]Argyris, J., "An Excursion into Large Rotations," *Computer Methods in Applied Mechanics and Engineering*, Vol. 32, No. 1–3, 1982, pp. 85–155.

[53]Spring, K. W., "Euler Parameters and the Use of Quaternion Algebra in the Manipulation of Finite Rotations: A Review," *Mechanism and Machine Theory*, Vol. 21, No. 5, 1986, pp. 365–373.

[54]Ibrahimbegovic, A., "On the Choice of Finite Rotation Parameters," *Computer Methods in Applied Mechanics and Engineering*, Vol. 149, No. 1–4, 1997, pp. 49–71.

[55]Batra, R. C., and Yu, J. H., "Linear Constitutive Relations in Isotropic Finite Viscoelasticity," *Journal of Elasticity*, Vol. 55, No. 1, 1999, pp. 73–77.

[56]ABAQUS/Standard User's and Theory Manuals, Ver. 5.8, Hibbitt, Karlsson, and Sorensen, Pawtucket, RI, 1998.

[57]Warriner, W. C., "Designing with Delrin," *Mechanical Engineering*, Vol. 81, No. 4, 1959, pp. 60–64.

[58]Rogers, T. G., and Lee, E. H., "On the Finite Deflection of a Viscoelastic Cantilever," *Proceedings of the 4th U.S. National Congress of Applied Mechanics*, American Society of Mechanical Engineers, New York, 1962, pp. 977–987.

[59]Seide, P., and Jamjoom, T. M. M., "Large Deformations of Circular Rings Under Nonuniform Normal Pressure," *Journal of Applied Mechanics*, Vol. 41, No. 1, 1974, pp. 192–196.

[60]Timoshenko, S., and Gere, J., *Theory of Elastic Stability*, 2nd ed., McGraw–Hill, New York, 1961, pp. 76–82.

[61]Hammerand, D. C., "Geometrically-Linear and Nonlinear Analysis of Linear Viscoelastic Composites Using the Finite Element Method," Ph.D. Dissertation, Dept. of Aerospace and Ocean Engineering, Virginia Polytechnic Inst. and State Univ., Blacksburg, VA, Sept. 1999.

[62]Wu, C. H., and Tauchert, T. R., "Thermoelastic Analysis of Laminated Plates. 2: Antisymmetric Cross-Ply and Angle-Ply Laminates," *Journal of Thermal Stresses*, Vol. 3, No. 3, 1980, pp. 365–378.

[63]Tauchert, T. R., "Thermal Buckling of Thick Antisymmetric Angle-Ply Laminates," *Journal of Thermal Stresses*, Vol. 10, No. 2, 1987, pp. 113–124.

A. N. Palazotto
Associate Editor